ChemPhysMater 5 (2026) 284–301

Contents lists available at ScienceDirect

ChemPhysMater

journal homepage: https://www.keaipublishing.com/en/journals/chemphysmater/

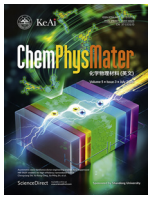

Review Article

Design of MXene-based composites for multimodal therapeutic applications

Shilong Fu[a], Huanyu Jin[b,*], Xu Xiao[a,*]

[a] School of Physics, University of Electronic Science and Technology of China, Chengdu 611731, China
[b] Institute of Technology for Carbon Neutrality, Shenzhen Institutes of Advanced Technology, Chinese Academy of Sciences, Shenzhen 518055, China

ARTICLE INFO

Keywords:
MXene-based composite
Multimodal therapy
Reactive oxygen species
Energy conversion and synergistic mechanisms

ABSTRACT

Multimodal therapeutic strategies that integrate photothermal therapy (PTT) with chemodynamic therapy (CDT), photodynamic therapy (PDT), and sonodynamic therapy (SDT) have been shown to generate synergistic therapeutic effects in biomedical applications. These synergistic effects significantly enhance treatment efficacy and offer promising approaches for the treatment of serious diseases such as tumors and drug-resistant bacterial infections. This review systematically summarizes the underlying mechanisms and energy conversion processes in PTT, CDT, PDT, and SDT that are responsible for tumor cell ablation and bacterial eradication. In particular, the unique advantages of MXene materials in integrating these distinct therapeutic modalities are presented. On this basis, recent advances in various MXene-based composite materials for multimodal therapy are also comprehensively reviewed. The structural design strategies, synergistic functionalities and performance advantages of different composite systems are highlighted. Finally, the challenges and opportunities associated with MXene-based materials in multimodal therapeutic applications are discussed. These discussions provide guiding insights for the rational design of this emerging class of nanomedicines, offering potential strategies for treating tumors and drug-resistant bacterial infections.

1. Introduction

The treatment of major diseases such as malignant tumors and infections caused by drug-resistant bacteria has long been confronted with substantial challenges, including limited therapeutic efficacy, pronounced systemic side effects, and the difficulty of overcoming complex pathological microenvironments [1,2]. Although a growing number of novel organic small-molecule drugs have been continuously discovered and translated into clinical application, their therapeutic outcomes are often constrained by relying on a single therapeutic mechanism [3,4]. In recent years, advanced nanomedicines have emerged as highly promising therapeutic agents in biomedical applications [5,6]. Owing to their multimodal therapeutic capabilities and synergistic mechanisms, these nanomaterial-based systems can integrate multiple treatment modalities—such as photothermal therapy (PTT), chemodynamic therapy (CDT), photodynamic therapy (PDT), and sonodynamic therapy (SDT)—to achieve spatiotemporally amplified therapeutic effects [7,8]. And the nanomedicines not only significantly enhance overall therapeutic efficiency but also mitigate the systemic toxicity associated with single-mode therapies [9,10]. Meanwhile, the unique size effects, interfacial characteristics, and tunable physicochemical properties of nanomedicines enable them to respond more effectively to external stimuli and adapt to complex pathological microenvironments [11]. Consequently, the rational construction of nanomedicine systems featuring multi-energy conversion capabilities and cooperative reaction pathways has attracted increasing attention from researchers.

Among various nanomedicines, 2D materials stand out as particularly promising candidates for multimodal therapy due to their unique physicochemical properties and versatile structural engineerability [7,12]. MXene as a class of emerging 2D materials composed of transition-metal carbides, nitrides, or carbonitrides have attracted considerable attention since their initial discovery [13,14]. Benefiting from the synergistic combination of metallically conductive frameworks and abundant surface functional groups, MXene exhibit outstanding electrical conductivity, high photothermal conversion efficiency, and excellent chemical stability [15,16]. Simultaneously, their intrinsic hydrophilicity and facile surface functionalization endow MXene with superior dispersibility and biocompatibility in complex physiological environments compared with conventional 2D materials and other inorganic materials. Within these composites, MXene can serve as efficient photothermal agents to generate localized heat, which not only directly induces tumor or bacterial cell ablation but also accelerates the reaction kinetics of reactive oxygen species (ROS) generation [17–22]. In parallel, their high electrical conductivity facilitates interfacial electron transfer and suppresses charge-carrier recombination, thereby significantly enhancing ROS production efficiency [23]. This integrated “carrier–nanoenzyme–

* Corresponding authors.
E-mail addresses: hy.jin2@siat.ac.cn (H. Jin), xuxiao@uestc.edu.cn (X. Xiao).

https://doi.org/10.1016/j.chphma.2026.03.001
Received 14 January 2026; Received in revised form 11 March 2026; Accepted 12 March 2026
Available online 14 March 2026
2772-5715/© 2026 The Authors. Publishing Services by Elsevier B.V. on behalf of KeAi Communications Co. Ltd. This is an open access article under the CC BY license (http://creativecommons.org/licenses/by/4.0/)

energy amplifier" synergistic mechanism endows MXene-based composites with markedly superior therapeutic performance in PTT–CDT, PTT–PDT, PTT–SDT, and other multimodal combination therapies compared with organic small-molecule drugs [24].

On this basis, this review systematically summarizes recent advances in MXene-based composite materials for multimodal biomedical therapy. Particular attention is given to the roles of MXene in energy conversion and reactive ROS generation, as well as to the design of composite systems that integrate metal oxides, metallic nanoparticles, single-atom nanoenzymes, metal coordination compounds, metal–organic frameworks (MOF), and metal peroxides. By comprehensively analyzing the advantages and limitations of different composite systems in CDT, PTT, PDT, SDT, and their combined therapeutic modalities, the unique advantages of various MXene-based composites are elucidated. This review aims to provide fundamental insights and rational design guidelines for the development and clinical translation of MXene-based multimodal therapeutic materials.

2. Overview of MXene and their potential in biomedical therapy

MXene is a class of two-dimensional layered materials composed of transition-metal carbides, nitrides, or carbonitrides, with a general formula of $M_{n+1}X_nT_x$, where M denotes a transition metal, X represents carbon or nitrogen, and T refers to surface functional groups such as hydroxyl (–OH), oxygen (–O), or fluorine (–F) [25]. Owing to their unique lamellar architecture and abundant surface terminations, MXene materials exhibit a variety of outstanding physicochemical properties, including remarkable electrical conductivity, high mechanical strength, and superior thermal and chemical stability. These characteristics collectively endow MXene with broad application potential in energy storage [26], catalysis [27], electronic device fabrication [28], and biomedical engineering [29]. In the field of biotherapy, the two-dimensional sheet-like structure and large specific surface area of MXene provide plentiful and uniformly distributed active sites for the efficient loading of drug molecules or nanoenzymes [13,30]. Additionally, their rich surface functional groups enable precise chemical modification, thereby enhancing targeting capability and overall biocompatibility in vivo [31]. These hydrophilic terminal groups also improve the dispersibility of MXene under physiological conditions, allowing them to maintain more stable and homogeneous suspensions in aqueous biological environments compared with other two-dimensional materials [32]. Additionally, the remarkable photothermal conversion efficiency of MXene enables them to facilitate synergistic interactions between CDT, SDT, PDT, and PTT, ultimately resulting in a multimodal therapeutic approach [33]. This tunable and multifunctional behavior positions MXene as highly promising candidates for constructing effective and controllable biotherapeutic platforms, while also providing new opportunities and research directions for the application of two-dimensional materials in multimodal therapy.

3. MXene-mediated energy conversion and cytotoxic mechanisms

3.1. Photothermal therapy

Photothermal therapy (PTT) utilizes materials with efficient photothermal conversion capabilities to transform light into heat, enabling localized thermal ablation of tumor cells or bacteria [34–36]. This photothermal process arises from a sequence of energy relaxation pathways during photoexcitation (Fig. 1). Upon irradiation, photons are absorbed by the material, promoting electrons from the ground state to higher energy levels and generating electron–hole pairs. In MXene materials with metallic characteristics or high carrier concentrations, light absorption can additionally occur via surface plasmon resonance. The resulting excited carriers rapidly couple with phonons and undergo nonradiative relaxation, producing heat and elevating the material's surface temperature [37,38]. Among available light sources, the NIR-I (650–950 nm) and NIR-II (1000–1350 nm) windows are particularly advantageous due to deeper tissue penetration, lower scattering, and reduced absorption by biological tissues. These properties enable efficient energy delivery to tumor or inflamed regions while minimizing damage to surrounding healthy tissues. Compared to conventional photothermal agents such as gold nanorods, graphene, and carbon nanotubes, MXene exhibit notable advantages in photothermal conversion efficiency, tissue penetration, surface functionalization, and thermal stability. For example, $Ti_3C_2F_x$ MXene can achieve photothermal conversion efficiencies exceeding 40%, and surface modifications can further approach theoretical limits [39,40]. This high efficiency is attributed to the high free-electron density, rapid relaxation of photoexcited electrons, and strong electron–phonon coupling in MXene, which collectively facilitate rapid heat generation via nonradiative transitions. Moreover, the two-dimensional sheet-like morphology provides a large specific surface area and enhanced interfacial interactions, further promoting light absorption and overall photothermal performance [41,42].

3.2. Chemodynamic therapy

Chemodynamic therapy (CDT) induces the generation of highly oxidative reactive oxygen species (ROS) within the cellular microenvironment via Fenton-like reactions [43,44]. These ROS cause irreversible damage to biomacromolecules, leading to cellular dysfunction, membrane rupture, and activation of mitochondrial apoptotic pathways, ultimately resulting in the elimination of tumor cells or bacteria. Mechanistically, ROS can oxidize polyunsaturated fatty acids in cell membranes, generating abundant lipid peroxidation products that compromise membrane fluidity, integrity, and permeability, thereby disrupting ion homeostasis and inducing membrane rupture—one of the key triggers of cell death. Concurrently, ROS can react with nucleic acids, causing base oxidation, single- or double-strand breaks, and DNA–protein crosslinking, which leads to genomic instability, cell cycle arrest, and activation of DNA damage response pathways and apoptosis [1,45]. Additionally, intracellular proteins are susceptible to radical-mediated oxidation, including side-chain modifications, backbone cleavage, or disruption of metal centers, resulting in enzyme inactivation, signaling dysregulation, and endoplasmic reticulum stress, ultimately contributing to cell death [46].

In CDT, ROS are generated through intracellular Fenton reactions. Taking Cu-catalyzed Fenton reactions as an example, the process can be described as follows (Fig. 1): $Cu^{2+} + H_2O_2 \rightarrow Cu^{+} + \cdot OOH + H^{+}$, $Cu^{+} + H_2O_2 \rightarrow Cu^{2+} + \cdot OH + OH^{-}$ [47]. During this process, divalent copper ions (Cu^{2+}) react with hydrogen peroxide (H_2O_2) to produce monovalent copper ions (Cu^{+}), superoxide radicals (HOO·), and protons (H^{+}). The resulting Cu^{+} subsequently reacts with H_2O_2 to generate hydroxyl radicals (·OH) and hydroxide ions (OH^{-}), establishing a catalytic Cu^{2+}/Cu^{+} cycle that continuously produces highly reactive ·OH, the strongest oxidant in the system, capable of eradicating tumor cells [48]. CDT relies on H_2O_2 generated from cellular metabolism and nanoenzymes with high Fenton activity.

Although the intrinsic Fenton catalytic activity of MXene is limited under conventional conditions, their unique physicochemical properties make them excellent platforms for supporting various nanoenzymes. The layered structure of MXene provides stable anchoring sites for semiconductor nanoenzymes, effectively preventing nanoparticle aggregation or deactivation during reactions, thereby enhancing the stability and reproducibility of the composite system [49]. Their abundant and tunable surface functional groups offer a versatile platform for subsequent chemical modification [50]. Furthermore, the inherent photothermal properties of MXene enable localized heating, which not only accelerates ROS generation but also enhances the reaction kinetics between ROS and biomacromolecules, promoting rapid oxidation of cellular membranes, proteins, and nucleic acids [51]. This synergistic effect amplifies apoptotic and necrotic

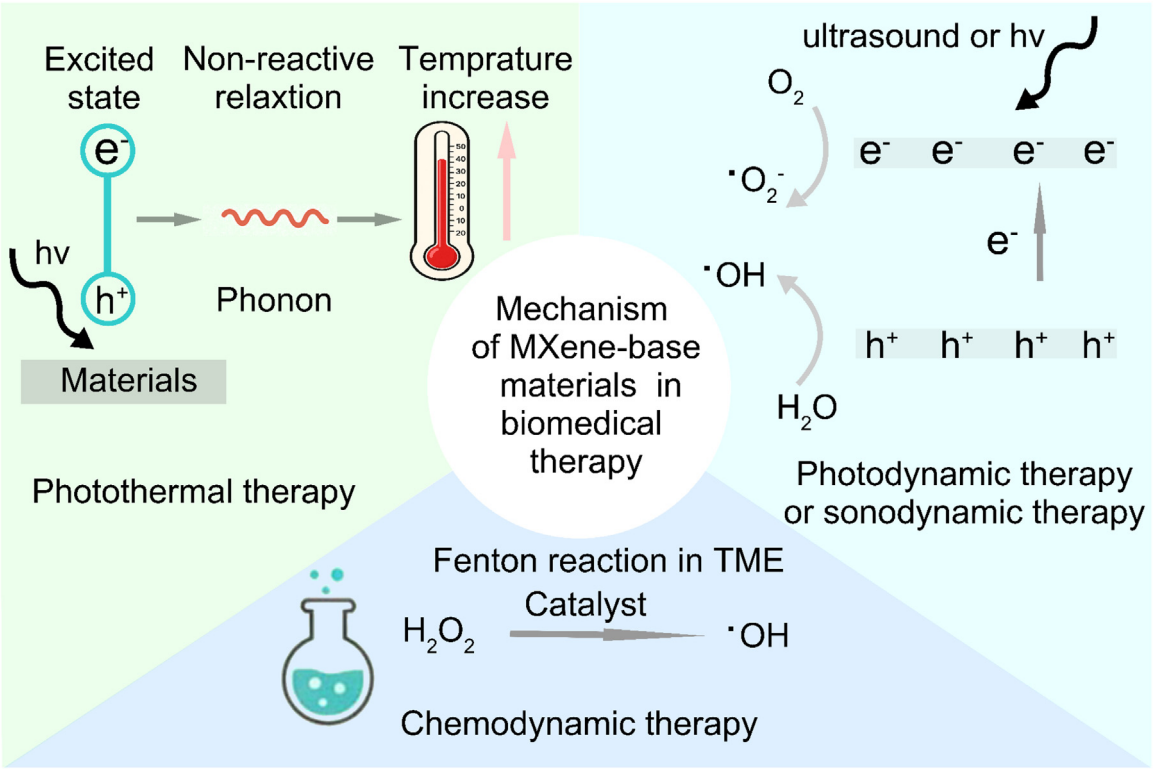

Fig. 1. Schematic diagram of mechanism of MXene-based materials in biomedical therapy.

processes, making MXene highly effective in PTT–CDT multimodal therapy.

3.3. Sonodynamic therapy and photodynamic therapy

Similar to CDT, sonodynamic therapy (SDT) and photodynamic therapy (PDT) exert their therapeutic effects primarily through the cytotoxic action of ROS against tumor cells or bacteria, with the underlying ROS-mediated mechanisms largely analogous to those in CDT [52,53]. However, the types of ROS and their generation pathways differ among these modalities. In CDT, the predominant ROS are hydroxyl radicals (·OH) and a minor fraction of hydroperoxyl radicals (·OOH), whereas SDT and PDT can generate a broader spectrum of ROS, including ·OH, superoxide radicals (O_2·$^-$), singlet oxygen ($^1O_2$) [5,6,54]. Within CDT, ROS originate from intracellular Fenton reactions catalyzed by suitable materials, requiring high Fenton catalytic activity. By contrast, ROS generation in SDT and PDT follows distinct mechanisms (Fig. 1). Two main pathways are involved: electron transfer and energy transfer. In the electron transfer pathway, the nanoenzyme undergoes electron excitation, producing electron–hole pairs. The excited electrons possess reducing ability and can convert O_2 to O_2·$^-$, while the holes oxidize H_2O to ·OH [55,56]. In the energy transfer pathway, the nanoenzyme gets energy and transitions from the ground state to the singlet excited state, which then undergoes intersystem crossing to a longer-lived triplet excited state. This triplet state acts as a key intermediate, transferring energy non-radiatively to surrounding ground-state triplet oxygen to generate highly reactive $^1O_2$ [57,58]. Although SDT and PDT share similar ROS generation principles, their energy conversion modes differ slightly. In PDT, nanoenzymes directly absorb photon energy, inducing electron excitation and hole formation, leading to ROS production [59,60]. In SDT, the quantum energy of ultrasound is insufficient for directly inducing electronic transitions. Consequently, cavitation serves as the dominant physical mechanism, responsible for triggering ROS generation. During ultrasound propagation in liquids, periodic negative pressures induce nucleation, growth, and oscillation of microbubbles. These bubbles collapse violently under extreme acoustic pressure, generating localized ultrahigh temperatures. The energy from these micro-hotspots can excite nanoenzyme electrons from the ground state, forming electron–hole pairs and promoting ROS production [61,62].

Nevertheless, most MXene are conductive materials. Even under surface plasmon resonance, the resulting excitations do not effectively produce ROS; thus, pure MXene are generally inactive in PDT and SDT. Despite this, MXene have found extensive application in SDT and CDT due to their unique physicochemical properties. Firstly, their excellent electrical conductivity facilitates rapid electron transfer at the interface between MXene and semiconductor nanoenzymes, significantly reducing carrier recombination and enhancing the separation efficiency of photo- or sono-generated electron–hole pairs [63,64]. Secondly, loading SDT or PDT nanoenzyme onto MXene prevents nanoenzyme aggregation and provides a platform for targeted delivery, similar to CDT strategies. Moreover, the intrinsic photothermal properties of MXene enable synergistic PTT effects in combination with PDT or SDT, further enhancing ROS-mediated cytotoxicity against tumor cells or bacteria [65,66]. Collectively, these features make MXene ideal platforms for constructing efficient multimodal therapeutic systems.

4. Advances in MXene-based composites

4.1. MXene–oxide composites

Oxide materials have demonstrated significant advantages in CDT in recent years, owing to their unique electronic structures and tunable surface chemistry. Many metal oxides possess adjustable metal valence states and abundant oxygen vacancies, which provide the necessary conditions for efficient participation in Fenton or Fenton-like reactions within the tumor microenvironment and infection microenvironment [67,68]. Benefiting from the active sites on the oxide surface and possible internal electron transport pathways, these materials can sustain internal electron transfer even under conditions of limited reductant availability, thereby maintaining stable valence cycling processes (e.g.,

Fe^{3+}/Fe^{2+}, Cu^{2+}/Cu^{+}) [69,70]. Such continuous valence cycling enables oxides to generate hydroxyl radicals (·OH) persistently, ensuring the stability and durability of the CDT process. Furthermore, oxides generally exhibit high lattice stability; their robust structural frameworks provide effective structural buffering under high ROS concentrations, preventing rapid deactivation and further ensuring sustained catalytic performance [71,72].

In MXene–oxide composite systems, the inherent advantages of valence cycling are further amplified. MXene exhibit pronounced photothermal responsiveness, enabling rapid temperature elevation under near-infrared (NIR) irradiation. According to the Arrhenius equation,which describes the temperature dependence of reaction rate constants and is expressed as:

$$k = A\exp\left(-\frac{E_a}{RT}\right),$$

where k is the rate constant, A is the pre-exponential factor, E_a is the activation energy, R is the universal gas constant, and T is the absolute temperature, the rate constant increases exponentially with increasing temperature. As temperature rises, a larger fraction of molecules has sufficient energy to overcome the activation barrier, leading to a positive correlation between temperature and reaction rate. This localized heating accelerates reaction kinetics, significantly enhancing ROS generation and thereby producing more pronounced PTT–CDT synergistic effects. Consequently, composites combining MXene with mixed-valence oxides have been widely reported and explored for multimodal therapeutic applications. For instance, Li et al. synthesized mixed-valence $Cu_{2-x}O$ containing both Cu_2O and CuO via ascorbic acid reduction, and subsequently constructed a $Ti_3C_2F_{2-x}/Cu_{2-x}O$ composite nanoenzyme (Figs. 2(a)(b)). The mixed-valence $Cu_{2-x}O$ efficiently and continuously generated ROS, while the excellent photothermal properties of $Ti_3C_2F_x$ enabled rapid temperature rise within a short period. Compared with control groups without NIR irradiation (Figs. 2(c)(d)), elevated temperatures accelerated ROS production, thereby enhancing the bactericidal activity of $Cu_{2-x}O$ under PTT–CDT synergistic conditions (Figs. 2(e)(f)) [73]. In addition to Cu-based oxides, Fe-based oxides as classical Fenton nanoenzymes have garnered sustained attention. Cai et al. incorporated spinel-structured $MnFe_2O_4$ into $Ti_3C_2F_x$ using chitosan as a chemical crosslinker. The composite retained a stable and pronounced photothermal response, while the mixed occupancy of tetrahedral and octahedral sites in $MnFe_2O_4$ naturally maintains a Fe^{2+}/Fe^{3+} mixed-valence state. This intrinsic property allows spontaneous Fenton cycling: Fe^{2+} reacts with H_2O_2 to generate ·OH, and Fe^{3+} is reduced back to Fe^{2+} by the tumor-abundant glutathione (GSH), sustaining continuous ROS production. When combined with NIR irradiation, the $Ti_3C_2F_x/MnFe_2O_4$ composite achieves markedly superior antitumor efficacy compared with either $Ti_3C_2F_x$ alone or the composite under non-photothermal conditions [74].

Meanwhile, beyond conventional Cu- and Fe-based oxides, which are traditionally recognized for their prominent Fenton or Fenton-like catalytic performance, increasing attention has been directed toward other metal oxides. These emerging materials also leverage valence modulation capabilities, tunable surface chemistry, and designable defect structures, offering unique advantages during H_2O_2 activation. Thereby, these materials can promote efficient generation of ROS due to enhanced electron transfer and optimized adsorption of reactants [75,76].

Among them, CeO_2 has emerged as a kind of representative materials with notable Fenton-like catalytic properties. The surface of CeO_2 is typically rich in oxygen vacancies, which serve as active sites that enable dynamic and reversible Ce^{4+}/Ce^{3+} valence cycling at the interface [77]. This valence flexibility facilitates rapid electron transfer during H_2O_2 decomposition, thereby accelerating the formation of hydroxyl radicals. Furthermore, the presence of surface defects not only reduces the reaction energy barriers but also stabilizes intermediate species, collectively enhancing the overall rate and efficiency of Fenton-like reactions [78,79] . Such insights highlight the potential of designing advanced metal oxide nanoenzymes with controlled defects and valence states to achieve superior ROS generation for applications in environmental remediation and catalytic therapeutics. Owing to these characteristics, CeO_2 and its derived systems have been widely investigated in biomedical catalysis and related fields, gradually emerging as an important branch of Fenton-like catalytic materials. For example, Wu et al. prepared nanoscale CeO_2 via a solvothermal method and integrated it with $Ti_3C_2F_x$. The Ce^{4+}/Ce^{3+} cycle enabled substantial ROS generation, and under additional NIR irradiation, the photothermal effect of $Ti_3C_2F_x$ increased the ·OH generation rate from 2.0×10^{-8} to 4.3×10^{-8} M s^{-1}, representing a 215% enhancement, quantitatively demonstrating the significant role of MXene-mediated photothermal effects in promoting ROS production. Consequently, this composite exhibited excellent tumor cell-killing efficacy [80]. Similarly, Yang et. al constructed $CeO_2/Ti_3C_2F_x$ composites via various synthesis methods. Although the number of surface defects in CeO_2 varied depending on the preparation route, it exhibited effective tumor suppression, further confirming the broad applicability and promising potential of CeO_2/MXene systems in cancer therapy [81].

Metal oxide materials also exhibit multiple distinctive advantages in PDT, primarily through unique electronic structures and tunable optical properties. Many metal oxides possess adjustable band structures, which can be effectively engineered via doping, defect modulation, or interfacial design to extend light absorption into the visible and NIR regions, thereby enhancing excitation efficiency. This band structure modulation redistributes internal electronic states, improving the separation and migration of photogenerated electron–hole pairs, reducing carrier recombination in the bulk and at the surface, and enabling more efficient ROS production under light irradiation, ultimately boosting PDT efficacy. For instance, Yang et al. synthesized vertically aligned TiO_2/MXene (v-TiO_2/MXene) composites. Owing to the unique interfacial structure between v-TiO_2 and MXene, charge transfer at the interface is significantly enhanced compared with parallel-aligned p-TiO_2/MXene. This leads to faster carrier migration, reduced electron–hole recombination, and improved adsorption and activation of oxygen and water molecules. Under simulated sunlight, v-TiO_2/MXene exhibited superior ROS generation relative to p-TiO_2/MXene, and combined with the intrinsic photothermal effect of MXene, demonstrated markedly enhanced antibacterial performance compared with both control systems [82]. Beyond conventional semiconductor–MXene heterostructures, compositional complexity can also be introduced to further modulate the electronic structure and carrier dynamics. Wu et al. prepared a high-entropy spinel oxide, $(CoCrFeMnNi)_3O_4$, via multicomponent doping (Fig. 3(a)). Variations in electronegativity and crystal field splitting among the 3d transition metals result in band broadening differences, yielding a narrower bandgap compared with lower-component oxides and enabling efficient NIR absorption. The high-entropy effect introduces substantial structural disorder, while strong intermetallic interactions induce valence electron fluctuations, whereby outer-shell electrons of the metal ions rapidly oscillate among multiple valence states (Fig. 3(b)). This dynamic behavior strengthens interfacial interactions with MXene, promoting efficient charge transfer at the heterointerface (Fig. 3(c)). Meanwhile, the continuous fluctuation of valence states provides additional pathways for electron exchange, further enhancing the conductivity and charge mobility within the composite system. As a result, the transferred electrons and holes at the interface between $(CoCrFeMnNi)_3O_4$ and MXene can be spatially separated more effectively, which significantly suppresses carrier recombination and prolongs the lifetime of the charge carriers. Under 808 nm NIR irradiation, the heterostructure interface exhibits high reactivity, generating abundant local ROS (Fig. 3(d)). Coupled with photothermal effect of MXene, the $(CoCrFeMnNi)_3O_4$/MXene composite demonstrates effective antibacterial performance under synergistic PTT–PDT treatment [83].

In SDT, the band structure of oxide materials also plays a critical role. The transient high temperatures, high pressures, and excitation events generated during acoustic cavitation rely on appropriately matched en-

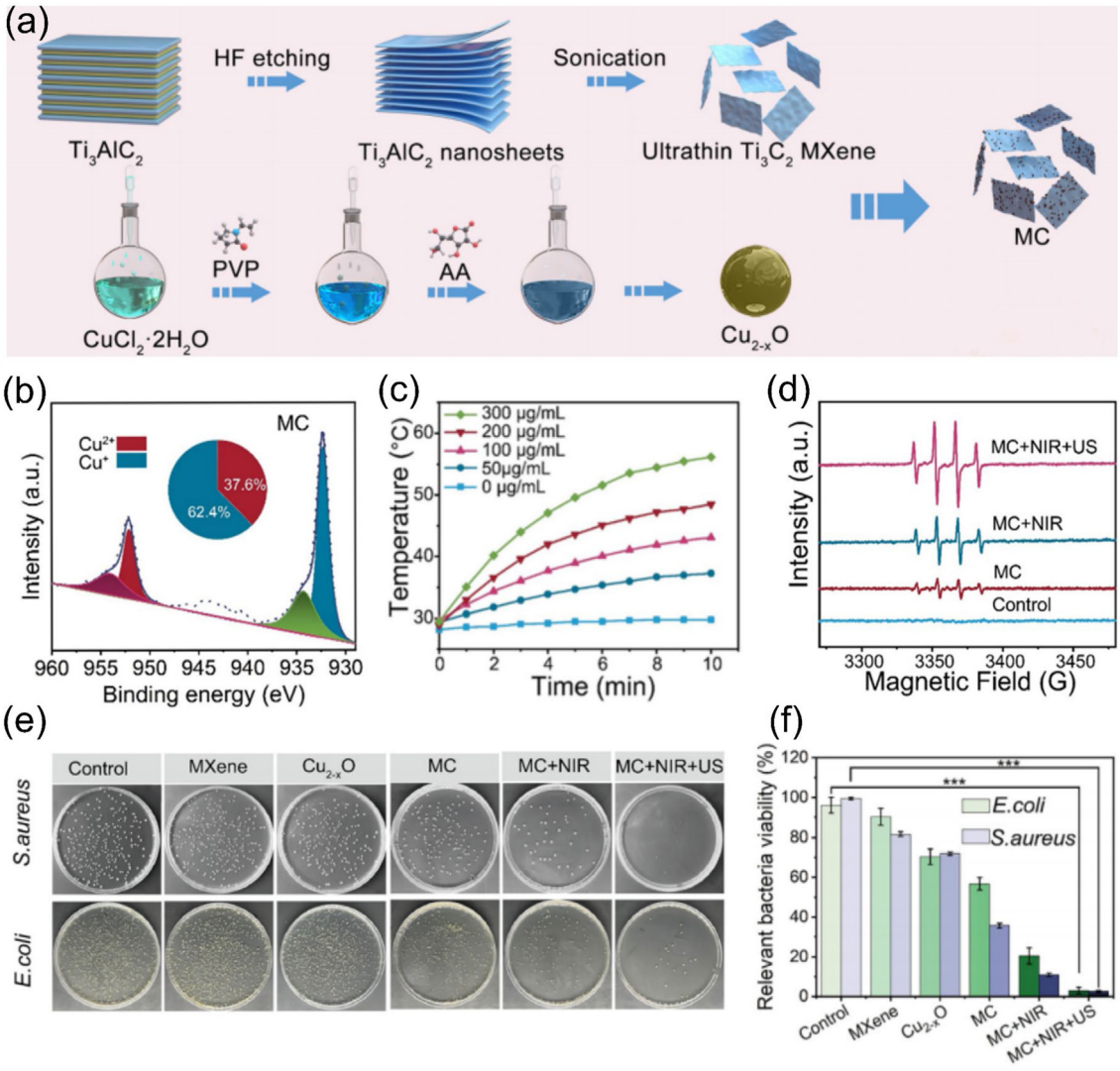

Fig. 2. (a) Schematic illustration of the synthesis process of $Cu_{2-x}O$/MXene; (b) multivalent copper states present in $Cu_{2-x}O$/MXene; (c) Photothermal performance under NIR irradiation; (d) Quantitative analysis of ROS generation in the Fenton reaction; (e)(f) Antibacterial activity of $Cu_{2-x}O$/MXene [73]. Copyright 2025 The Royal Society of Chemistry.

ergy levels to effectively convert sonically induced excitation into ROS generation. Oxides, with their tunable band structures, enable efficient electron excitation, migration, and separation under sonication, thereby achieving high-efficiency conversion of acoustic energy into chemical energy [85,86]. Furthermore, surface defects, such as oxygen vacancies, can act as "hotspot trapping centers," thereby significantly enhancing the efficiency of cavitation-induced mechanical excitation and endowing the materials with superior energy conversion performance under ultrasonic stimulation [87]. For example, Lin et al. employed hydrazine reduction to synthesize $TiO_x/Ti_3C_2F_x$ composites rich in oxygen vacancies. The abundant vacancies effectively modulated the band structure, reducing the bandgap to 2.65 eV, substantially lower than the intrinsic ~4 eV (Fig. 3(e)). Although NIR irradiation is insufficient to directly drive photoexcitation in $TiO_x/Ti_3C_2F_x$, the bandgap modulation facilitates electron excitation under ultrasonic cavitation, generating abundant excited electrons and holes, thereby markedly enhancing ROS production (Figs. 3(f)(g)). Meanwhile, the inherent photothermal effect of $Ti_3C_2F_x$ under NIR further amplifies the overall energy conversion, enabling $TiO_x/Ti_3C_2F_x$ to achieve efficient tumor ablation within an SDT–PTT multimodal framework [84]. Similarly, Cao et al. synthesized $TiO_2/Ti_3C_2F_x$ via in situ ultrasonic oxidation with tunable TiO_2 particle size, enabling bandgap modulation through defect engineering. The smallest composite exhibited a narrowed bandgap (2.37 eV), enhanced sonication-induced carrier separation, and improved ROS generation. Meanwhile, synergistic coupling of TiO_2-based SDT with the MXene photothermal effect also led to amplified ROS-mediated cytotoxicity and superior tumor therapeutic efficacy under SDT–PTT treatment [88].

Finally, oxide materials benefit from well-established and scalable synthetic protocols, providing clear advantages for engineering and biomedical applications. Large-scale, reproducible, and highly uniform production can be achieved via a variety of methods, including solvothermal reactions, thermal decomposition, self-assembly, co-precipitation, vapor deposition, and spray drying [89–92]. The controllability of these techniques allows precise tuning of precursor composition, reaction temperature, solvent environment, ligand system, and post-treatment processes, enabling systematic control over particle size, crystal phase, specific surface area, and exposed crystal facets [93,94]. Moreover, different synthetic strategies can introduce the key structural features, such as tunable oxygen vacancies, metal defects, surface coordinative unsaturation, and interfacial heterostructures. Through such structural engineering, catalytic performance can be finely optimized at

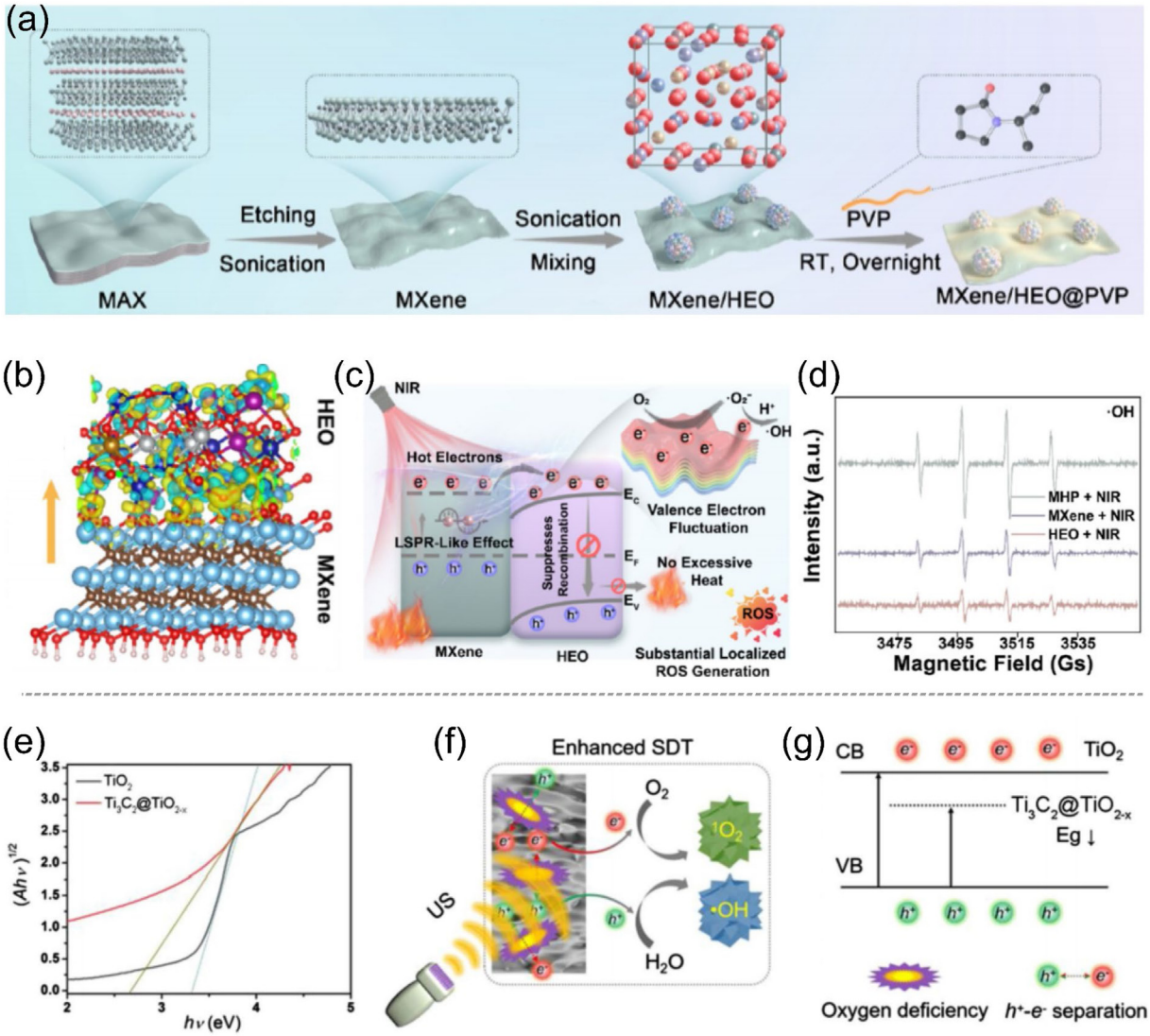

Fig. 3. (a) Schematic illustration of the synthesis of HEO/MXene; (b) Charge transfer of HEO/MXene; (c) band structure of HEO/MXene; (d) Quantitative analysis of ROS generation for MXene, HEO, and HEO/MXene [83]. Copyright 2025 American Chemical Society. (e) Band gap variation of TiO_{2-x}/Mxene; (f) Schematic illustration of the SDT process of TiO_{2-x}/MXene; (g) band structure of TiO_{2-x}/Mxene [84]. Copyright 2022 Springer Nature.

multiple levels, including active site density, electronic structure modulation, and reduction of reaction energy barriers, resulting in oxides that exhibit stable and efficient catalytic behavior across SDT, PDT, CDT, and other therapeutic mechanisms [95,96]. Importantly, many metal oxides have been demonstrated to possess favorable biocompatibility, allowing controlled degradation in vivo and subsequent clearance via hepatic or renal pathways. This minimizes potential long-term systemic toxicity, further underscoring their suitability for biomedical applications.

4.2. MXene–metal composites

4.2.1. MXene-nanoparticle composites

Although metal nanoparticles (NPs) cannot undergo the conventional Fenton cycle driven by valence variation, they can generate ROS via electron-transfer-mediated Fenton-like reactions when combined with certain functional materials. Owing to their unique physicochemical properties, have demonstrated significant potential in CDT [97,98]. Their advantages primarily stem from the high surface-to-bulk ratio so that they have abundant low-coordinated surface atoms inherent to the nanoscale, which create highly exposed and reactive sites capable of efficiently catalyzing H_2O_2 decomposition [99]. In the typically acidic and H_2O_2-rich microenvironment, these metal NPs can substantially lower the energy barrier for H_2O_2 cleavage into ROS [100]. In addition, the intrinsic high electron density and continuous electronic band structure of metal NPs facilitate rapid interfacial electron transfer, maintaining elevated electron flux at the reaction interface and further enhancing ROS generation, thereby providing kinetic support for the CDT effect [101]. However, owing to their large specific surface area, the surface energy of metal nanoparticles is correspondingly high, which readily leads to particle aggregation and a consequent decline in catalytic performance. Therefore, in practical applications, metal nanoparticles are typically supported on suitable substrates, where interactions between the metal and the carrier maintain high nanoparticle dispersion, ensuring stable and sustained catalytic activity [102].

Analogous to the synergistic effects observed in oxide/MXene systems, metal nanoparticle/MXene composites combine the excellent photothermal properties of MXene with the high reactivity of metal nanoparticles, making them widely applicable in multimodal therapeutic strategies. In addition to their high ROS-generating activity, metal nanoparticles also exhibit other biochemical reactivities beneficial for biotherapy, thereby providing additional synergistic therapeutic effects when integrated with CDT–PTT. Based on this design principle, Chen

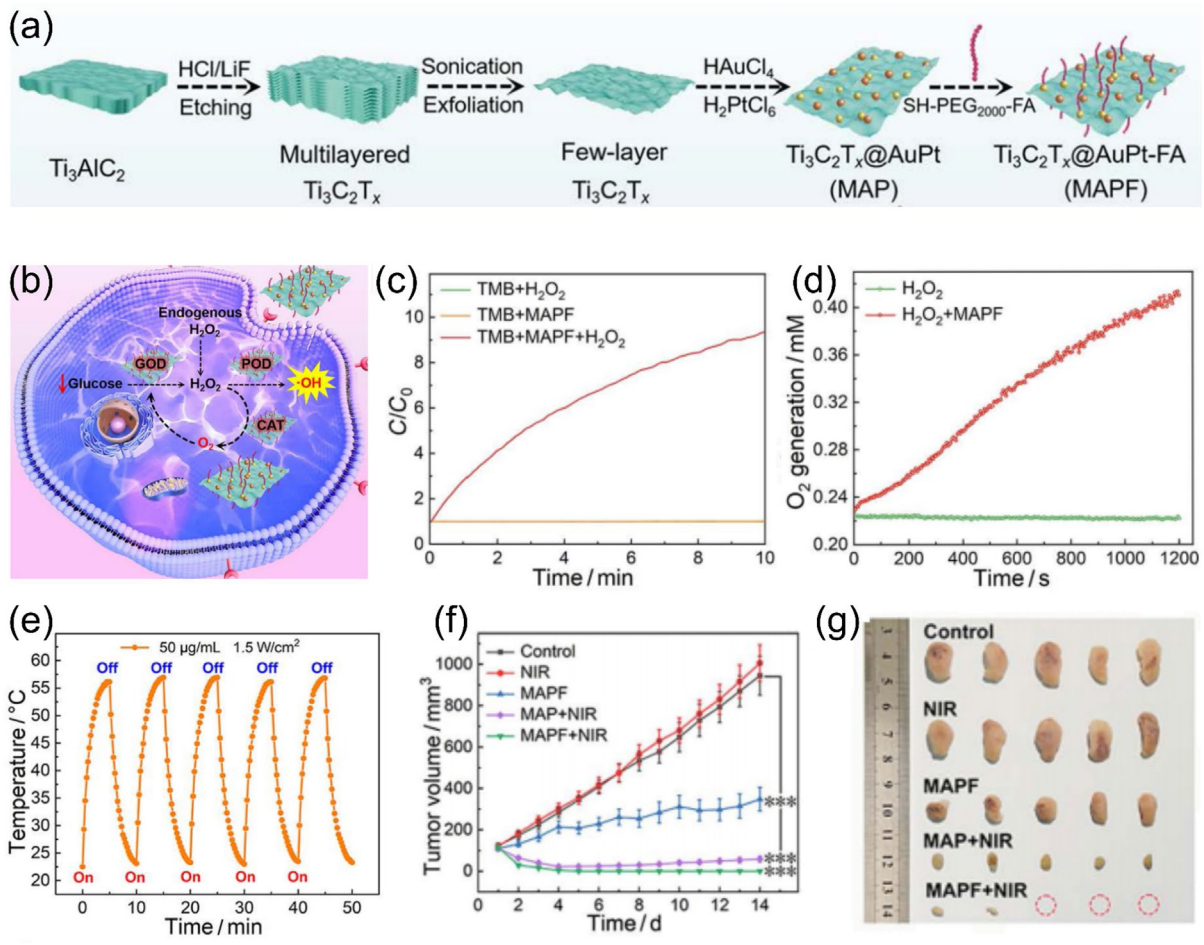

Fig. 4. (a) Schematic illustration of the synthesis of $Ti_3C_2T_x$@AuPt-FA; (b) The multifunctional of $Ti_3C_2T_x$@AuPt-FA; (c) ROS generation capability and (d) O_2 release capability of $Ti_3C_2T_x$@AuPt-FA; (e) Photothermal effect of $Ti_3C_2T_x$@AuPt-FA; (f)(g) Tumor therapeutic efficacy of $Ti_3C_2T_x$@AuPt-FA [104]. Copyright 2025 Wiley-VCH.

et al. loaded Pt nanoparticles onto MXene, generating a composite with both photothermal responsiveness and multifunctional catalytic activity. Under NIR irradiation, the material rapidly heats, enhancing active site exposure and ROS generation efficiency. Moreover, Pt nanoparticles also catalyze intracellular H_2O_2 decomposition and oxygen release, effectively alleviating tumor hypoxia. The generated oxygen also suppresses HIF-1α-mediated malignant phenotypes, partially relieving the immunosuppressive tumor microenvironment. Through combined multiple mechanisms, the Pt/MXene composite exhibits markedly improved antitumor efficacy under CDT–PTT synergistic therapy [103]. Similarly, Han et al. fabricated AuPt alloy nanoparticles supported on $Ti_3C_2T_x$, yielding a AuPt/$Ti_3C_2T_x$ composite with photothermal and multifunctional catalytic properties (Figs. 4(a)(b)). Under NIR irradiation, the synergistic interaction between Au and Pt results in a radical generation rate of 1.78×10^{-7} M s^{-1}, substantially higher than that of Au/$Ti_3C_2T_x$ (1.09×10^{-7} M s^{-1}) and Pt/$Ti_3C_2T_x$ (8.45×10^{-8} M s^{-1}), indicating enhanced ROS production efficiency in the composite (Fig. 4(c)). Additionally, this catalytic system mimics glucose oxidase activity, continuously oxidizing intracellular glucose at metal sites to generate endogenous H_2O_2, which further fuels sustained ROS production, establishing a stable and prolonged radical supply (Fig. 4(d)). Coupled with the exceptional photothermal amplification of MXene (Fig. 4(e)), the AuPt/$Ti_3C_2T_x$ composite achieves superior overall therapeutic performance under CDT–PTT multimodal therapy (Figs. 4(f)(g)) [104].

Based on the aforementioned studies, alloyed metal nanoparticles exhibit superior structural and electronic complementarity compared with monometallic systems, enabling the integration of multiple therapeutic mechanisms and significantly enhancing overall reaction efficiency [105]. Within the alloy framework, different metal elements leverage their unique catalytic activities, electronic structure, and surface adsorption characteristics to achieve synergistic functional cooperation. This allows the composite system to sustain efficient generation of ROS or other active species under the combined action of photothermal, chemodynamic, and sonodynamic modalities, even within complex microenvironments [106]. Moreover, the synergistic interactions among the metal components enables precise modulation of the system in response to various microenvironmental factors [107]. Consequently, alloy-based systems provide enhanced stability, prolonged functional duration, and significantly improved overall therapeutic performance, offering a reliable material foundation and strategic platform for multimodal therapy in complex biological systems [108,109]. For instance, Zheng et al. employed a hydrothermal method to load RuRh alloy nanoparticles onto $Ti_3C_2T_x$. The resultant nanoenzyme benefits from pronounced electron transfer interactions among Rh, Ru, and $Ti_3C_2T_x$, which enhance H_2O_2 adsorption and thereby effectively boost CDT activity. Additionally, the RhRu/$Ti_3C_2T_x$ system functions as a photosensitizer, converting O_2 to $\cdot O_2^-$ under NIR irradiation. Coupled with the intrinsic photothermal properties of the material, this composite integrates CDT, PDT, and PTT modalities, demonstrating excellent therapeutic efficacy against osteosarcoma. These findings further highlight the high multifunctionality and broad application potential of alloyed metal nanoparticles in multimodal tumor therapy [110].

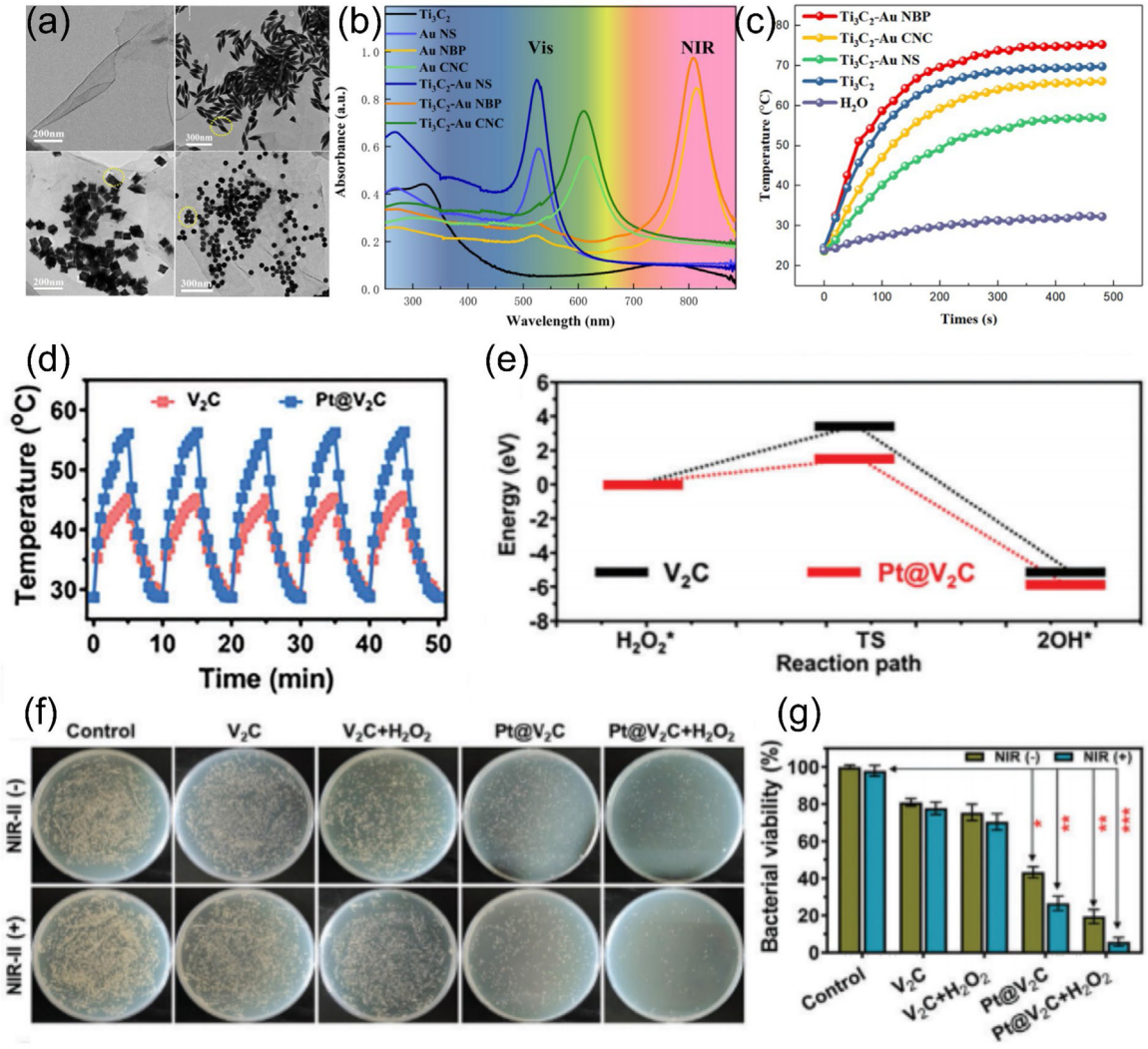

Fig. 5. (a) Au nanoparticles with different morphologies loaded on $Ti_3C_2T_x$; (b) enhancement ranges of light absorption of $Ti_3C_2T_x$ induced by Au nanoparticles with different morphologies; (c) Au-enhanced photothermal effects under near-infrared irradiation [116]. Copyright 2023 American Chemical Society. (d) enhancement of the photothermal effect by Pt; (e) Pt-enhanced Fenton reaction; (f)(g) antibacterial performance [117]. Copyright 2024 Wiley-VCH.

Metallic nanoparticles also exhibit significant photothermal enhancement in CDT due to their unique optical properties [111]. The key physical mechanism underlying this effect is localized surface plasmon resonance (LSPR), in which high-density free electrons in the metal collectively oscillate under light irradiation and rapidly convert photon energy into localized heat via nonradiative decay. This mechanism endows metallic nanoparticles with highly efficient photothermal conversion capabilities. Noble metals such as gold and silver, as well as certain metals with strong electron–phonon coupling, exhibit pronounced LSPR responses in the visible and near-infrared (NIR) regions, enabling rapid and controllable local heating [112,113]. Tailoring the size, morphology, and internal structure of metallic nanoparticles—such as via hollow, core–shell, or anisotropic designs—significantly modulates their LSPR behavior. This optimization enhances the light absorption cross-section, enabling effective optical triggering within the NIR-I and NIR-II biological windows [114,115]. This significantly improves their potential in antibacterial and anticancer applications. For example, Jiang et al. systematically varied the morphology of gold nanoparticles to produce nanoplates, nanocages, and nanorods (Fig. 5(a)). Distinct plasmonic absorption peaks were observed in the visible–NIR region for these structures: approximately 529 nm for nanoplates, 615 nm for nanocages, and 815 nm for nanorods (Fig. 5(b)). The latter falls within the NIR window with optimal tissue penetration, enabling efficient photothermal conversion at relatively low light intensities. When these gold nanorods were integrated with MXene, which possesses exceptional optoelectronic and photothermal responsiveness, both light absorption and photothermal effects were further amplified (Fig. 5(c)). Under NIR irradiation, the Au/MXene composite generates localized high temperatures more rapidly, thereby exhibiting superior photothermal antibacterial performance [116]. Furthermore, the plasmonic-mediated PTT of metal nanoparticles can synergize with their CDT activity, forming a multimodal PTT–CDT therapeutic platform with enhanced antitumor or antibacterial efficacy. For instance, Zhang et al. successfully loaded Pt nanoparticles onto V_2CT_x to construct a Pt/V_2CT_x composite nanoenzyme. Under NIR irradiation, the LSPR effect of Pt significantly enhanced the photothermal conversion efficiency of the system to 59.6%, compared with 29.6% for bare V_2CT_x (Fig. 5(d)). Meanwhile, the composite retained excellent catalytic activity in ROS generation (Fig. 5(e)). The pronounced photothermal effect also amplified CDT performance, resulting in superior antibacterial efficacy under the PTT–CDT multimodal strategy (Figs. 5(f)(g)) [117]. Similarly, Fang et al. loaded AgPd alloy nanoclusters onto $Ti_3C_2T_x$; these AgPd clusters exhibited strong LSPR under 808 nm NIR irradiation, enhancing the photothermal effect of the composite

and further boosting CDT activity, thereby achieving effective bacterial eradication [118].

Moreover, metallic nanoparticles exhibit highly engineerable structures and surface chemistries, allowing precise modulation of their growth kinetics during synthesis and enabling fine-tuned design and functionalization of multiple key parameters. Specifically, various strategies can be employed to achieve targeted performance optimization: for instance, controlling particle size and morphology (e.g., spherical, rod-like, cubic, or dendritic) to adjust surface area and surface energy; selectively exposing specific crystal facets to increase the density of highly active catalytic sites; or constructing complex core–shell or alloy architectures to realize synergistic effects among different metal components [119,120]. These deliberate structural designs aim to maximize the catalytic performance of the nanoparticles, particularly their enzyme-mimetic activity, allowing efficient catalysis of H_2O_2 via Fenton or Fenton-like reactions within tumor or bacterial microenvironments to generate abundant cytotoxic hydroxyl radicals [105,121]. Precisely engineered nanoenzyme can thus adapt to complex and challenging microenvironments—such as acidic pH, elevated H_2O_2 concentrations, and hypoxia—while maintaining high activity and stability [122,123]. Consequently, functionalized metallic nanoparticles have emerged as indispensable platforms for constructing next-generation, highly efficient, and low-side-effect CDT systems.

4.2.2. MXene-single atom

In recent years, single-atom nanoenzymes (SACs) as novel catalytic systems in which transition metal active sites are atomically dispersed on a support, have attracted considerable attention. Theoretically, SACs offer 100% atomic utilization, which not only enhances catalytic efficiency but also significantly reduces the usage of precious metals, thereby lowering overall nanoenzyme cost [124–126]. As a result, SACs have been widely explored for biomedical applications. MXene, characterized by high electrical conductivity, abundant surface termination groups, and controllable layered structures, provide robust coordination sites for anchoring single metal atoms [127,128]. Moreover, the intrinsic photothermal effect of MXene, coupled with efficient charge transfer, further enhances ROS generation. MXene can also modulate the valence states and d-orbital occupancy of the metal centers through interfacial electronic coupling, thereby promoting the electron transfer processes essential for Fenton or Fenton-like reactions [129]. Under MXene regulation, single-atom metal centers typically adopt low-coordination and unsaturated electronic structures, exhibiting enhanced H_2O_2 adsorption and activation capabilities, which substantially lowers the energy barrier for $H_2O_2 \rightarrow \cdot OH$ conversion and enables efficient ROS generation within the mildly acidic microenvironment (tumor microenvironment and infection microenvironment) [130,131]. Consequently, metal/MXene single-atom nanoenzymes represent an ideal platform for constructing highly efficient CDT systems. For example, He et al. synthesized a $Pt_1/Ti_3C_2O_2$ single-atom nanoenzyme with a Pt loading as low as 1 wt%. Even at this low loading, significant modulation of the material's band structure was observed, leading to excellent ROS production. When combined with the photothermal effect of $Ti_3C_2O_2$, the $Pt_1/Ti_3C_2O_2$ system demonstrated superior bactericidal performance under CDT–PTT dual-modal treatment [132]. Similarly, Jin et al. developed a Pt_1/Nb_2CT_x single-atom nanoenzyme with an extremely low Pt loading. The interfacial electronic interaction between Pt and Nb in the MXene substrate resulted in a mixed valence state of Pt^0/Pt^{2+}, which exhibited remarkable CDT activity. Coupled with the photothermal effect of Nb_2CT_x, this system achieved excellent synergistic CDT–PTT bactericidal performance [133].

4.3. MXene–metal coordination complex composites

4.3.1. MXene–molecular coordination complex hybrid composites

Metal coordination compounds exhibit unique and remarkable advantages in CDT, owing to the presence of catalytically active metal centers combined with precisely tunable ligand environments. Compared with traditional metal ions or metal oxide systems, coordination compounds enable fine modulation of the metal centers oxidation state and d-orbital configuration through electron-donating or -withdrawing effects of the ligands [134,135]. This tunability significantly lowers the activation barrier for H_2O_2 decomposition and enhances ·OH generation efficiency. For example, Wen et al. systematically demonstrated that the electronic structure of Fe centers in FeN_4 coordination environments is highly dependent on the type of nitrogen donor. The shift in the d-band center plays a crucial role in influencing the catalytic performance of FeN_4 sites. When the d-band center is positioned higher, as in the case of pyrrolic nitrogen compared to pyridinic nitrogen, it leads to a stronger overlap between the metal's d-orbitals and the electronic states of the adsorbate. This results in stronger adsorption of intermediates like H_2O_2, which can enhance the overall reactivity of the catalytic sites. Moreover, this shift can optimize reaction pathways, reduce activation energies, and promote the stability of the active catalytic sites (Figs. 6(a)(b)). This facilitates the formation and conversion of reactive intermediates, resulting in accelerated ROS production (Fig. 6(c)). Consequently, pyridinic-N coordinated FeN_4 sites exhibit superior therapeutic efficacy in vivo, outperforming other ligand configurations [136]. Building on this mechanism, the CoPc–Mn/$Ti_3C_2T_x$ system reported by Zhang et al. incorporates CoN_4 sites where all nitrogen donors originate from pyrrolic nitrogen (Fig. 6(d)). Such coordination engineering effectively enhances the electronic activity of the metal center and further promotes ROS generation. Moreover, the MXene substrate provides robust and pronounced photothermal effects, enabling enhanced tumor ablation through the synergistic combination of CDT and PTT (Figs. 6(e)(f)) [137]. In addition, certain ligands possessing intrinsic redox activity or photosensitivity can further cooperate with the metal centers, jointly participating in continuous electron-transfer processes. During reaction, these ligands not only help construct more efficient electron pathways in coordination with the metal sites but can also be photoexcited under irradiation or external stimuli, thereby significantly boosting ROS generation. For instance, in the MXene@ZnPcTa/CS system developed by Deng et al., the precisely engineered ligand exhibits strong NIR absorption and maintains stable photosensitizing activity upon excitation. Simultaneously, the photothermal effect arising from the MXene substrate is activated under irradiation, enabling synergistic PDT–PTT performance. Benefiting from the dual-mode mechanism, this nanoenzyme demonstrates pronounced antibacterial efficacy, highlighting the importance of structural design and functional cooperation [138]. Furthermore, the organic ligands of coordination compounds can bond with MXene and act as surface terminations, thereby enabling more robust integration with the MXene substrate [139] . This structural stabilization effectively suppresses rapid hydrolysis, precipitation, or biomolecule-induced deactivation of metal ions under physiological conditions. This ensures sustained and controllable catalytic activity within the mildly acidic tumor microenvironment, thereby improving the practical therapeutic efficiency of CDT. For example, Hao et al. coordinated Ru with 2,2′-bipyridine, followed by covalent assembly of the Ru complex onto the $Ti_3C_2T_x$ surface via reactions with surface functional groups, forming a Ru@MXene nanocomposite. This hybrid material exhibits excellent light absorption and a pronounced photothermal effect derived from the MXene substrate, thereby enabling synergistic CDT–PTT antibacterial performance. Importantly, the covalent bonding between the Ru complex and MXene—rather than simple van der Waals interactions—greatly enhances the structural stability of the composite [140].

4.3.2. MXene-metal organic frameworks hybrid composites

In addition to conventional molecular coordination complexes, metal organic frameworks (MOF) have recently attracted substantial attention as emerging platforms in biomedical catalysis. MOF are crystalline porous materials constructed through the self-assembly of metal ions or and multidentate organic ligands via coordination bonds [142,143].

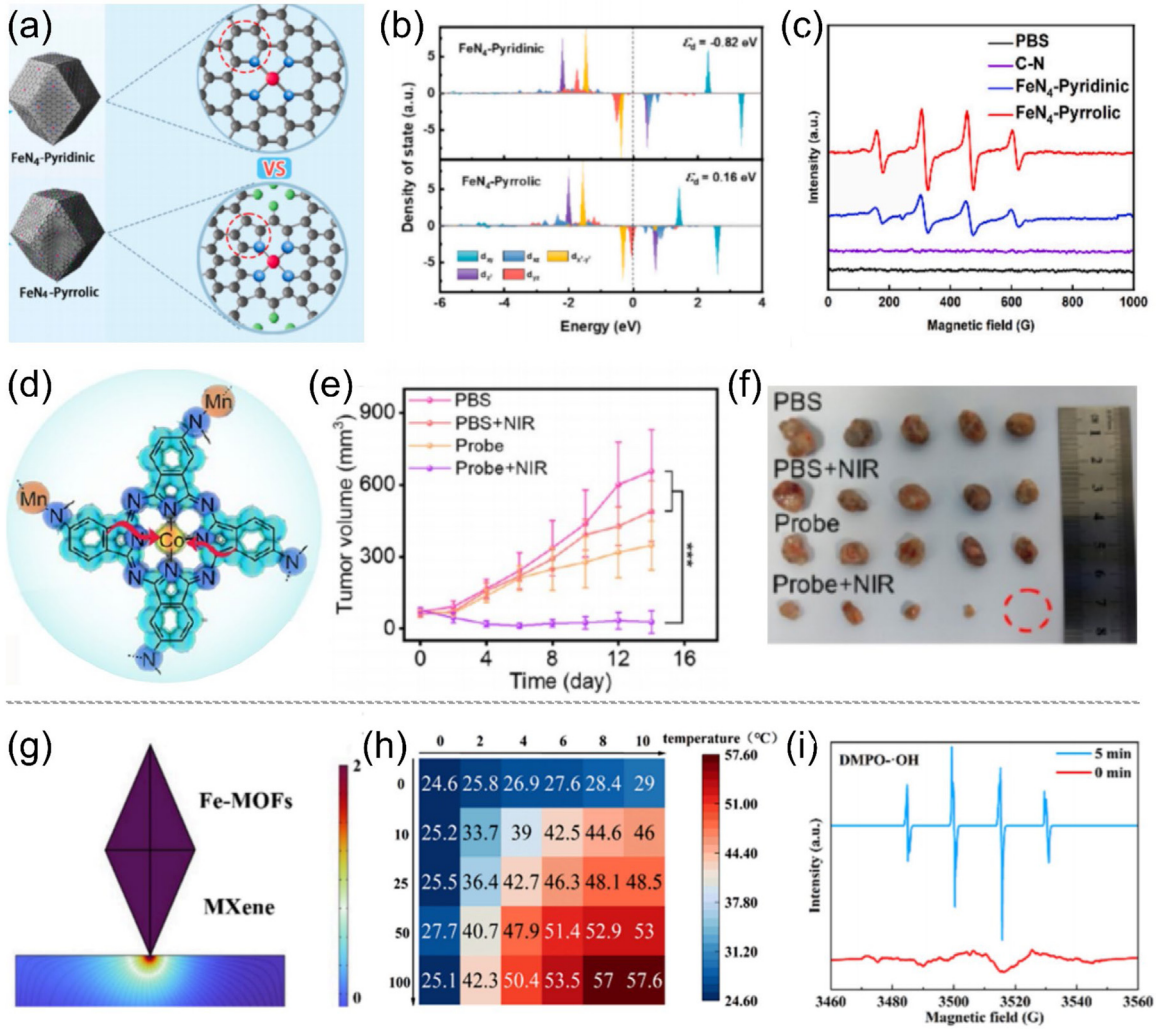

Fig. 6. (a) Schematic illustrations of Fe complexes with different coordination environments; (b) Effects of ligand coordination on the electronic structure of Fe centers; (c) Comparison of ROS generation capabilities of Fe complexes with different coordination structures [136]. Copyright 2025 Elsevier. (d) Structural illustration of a pyrrolic N–coordinated Co complex; (e)(f) Antitumor therapeutic performance of the pyrrolic N–coordinated Co complex [137]. Copyright 2025 American Chemical Society. (g) Visualization of the electric field distribution in the Fe-MOF/MXene hybrid under 808 nm laser irradiation; (h) Photothermal performance of the Fe-MOF/MXene hybrid; (i) ROS generation capability of the Fe-MOF/MXene hybrid [141]. Copyright 2025 American Chemical Society.

Owing to their highly designable node–linker topologies, MOF typically exhibit exceptionally high surface areas, tunable pore sizes, diverse chemical compositions, and outstanding structural engineerability [144]. By rationally selecting metal centers, tailoring ligand structures, or introducing defects and functional sites, the electronic structure, catalytic activity, and stability of MOF can be precisely modulated, making them an attractive class of materials for biomedical applications in recent years [145]. In the context of CDT, the advantages of MOF stem from several key features. First, MOF provide abundant and highly accessible metal active sites, enabling metal centers to efficiently participate in Fenton and Fenton-like reactions, thereby catalyzing the decomposition of endogenous H_2O_2 into ROS. Incorporation of different metal nodes such as Fe or Cu allows precise modulation of catalytic activity and redox cycling [144]. Second, the intrinsic porous channels of MOF provide high a specific surface area, thereby greatly facilitating the diffusion and interaction of reactant molecules within the framework and contributing to enhanced reaction kinetics and catalytic efficiency. Third, tuning metal atom species, creating lattice vacancies, or introducing electron-donor/acceptor moieties enhance electron transport, lower reaction barriers, and further boost ROS generation [146]. Moreover, the structural characteristics of MOF enable seamless integration with MXene to construct multifunctional platforms capable of synergistic CDT, PTT, and even PDT, thereby achieving significantly improved therapeutic outcomes. For instance, Yang et al. synthesized Fe-MOF via coordination between Fe ions and terephthalic acid (BDC), followed by hybridization with MXene to form Fe-MOF/MXene composites. Under NIR irradiation, a notable electric field intensity is generated within the MXene layer situated beneath the Fe-MOF structure. The distribution of the electric field within the MXene layer reveals a clear enhancement in the interfacial electron generation due to the presence of Fe-MOF. Additionally, the intrinsic photothermal properties of MXene, which exhibit significant heat generation upon NIR exposure, play a crucial role in augmenting this process. These factors synergistically contribute to the substantial generation of ROS, which are critical for the enhanced therapeutic efficacy. The interaction between the Fe-MOF and MXene layers under NIR exposure thus fosters a highly reactive environment conducive to ROS production, enabling advanced therapeutic potential (Figs. 6(g)–(i)), resulting in remarkable antibacterial performance under synergistic CDT–PTT treatment [141]. Similarly, Ke et al. coordinated Cu with tetrakis(4-carboxyphenyl)porphyrin (TCPP) to obtain a two-dimensional Cu-TCPP MOF and further integrated it with MXene to construct Cu-TCPP/$Ti_3C_2F_x$ composites. With highly active Cu

sites, strong photo absorption of TCPP, and MXene-induced photothermal amplification, this system exhibited outstanding antibacterial performance under multimodal CDT–PDT–PTT therapy, along with effective inflammation suppression in vivo [12]. Overall, the programmable architecture, efficient utilization of metal sites, and compatibility with multimodal therapeutic strategies collectively position MOF as highly functional and adaptable platforms for CDT. Their structural versatility and microenvironment responsiveness endow MOF with significant advantages and broad prospects for advanced tumor therapy applications.

Overall, the integration of metal coordination compounds with MXene gives rise to an efficient catalytic system that combines tunable electronic structures, pronounced photothermal responsiveness, and robust interfacial stability [147]. Through ligand engineering, the metal centers can be precisely modulated in terms of valence state, thereby markedly enhancing their ability to activate H_2O_2 [148]. Meanwhile, MXene, with its excellent electrical conductivity and photothermal properties, further accelerates electron transfer and enables the construction of multiple synergistic therapeutic mechanisms. In addition, the intrinsic photosensitivity or redox activity of the ligands, the structural stability of MXene, and the strong interfacial interactions formed within the composite collectively enhance the sustained catalytic behavior of the material under the weakly acidic microenvironment [149]. At the same time, MOF—as another highly designable class of coordination systems—offer further advantages when integrated with MXene. The combination not only improves the utilization efficiency of metal nodes and amplifies the mass transport benefits arising from the porous framework, but also enables deeper synergy among CDT, PTT, and even PDT, thereby providing a more versatile strategy for constructing multimodal therapeutic platforms [150]. Taken together, whether based on molecular coordination complexes or MOF, their hybridization with MXene provides systematic structural support for enhancing catalytic activity, strengthening photothermal and photosensitized responses, and improving interfacial stability. As a result, metal coordination compound/MXene composites demonstrate substantial potential for applications in both tumor therapy and antibacterial treatment.

4.4. MXene-peroxide composites

Metal peroxides have attracted increasing attention in the field of CDT in recent years, primarily due to their unique “self-supplying” ROS generation characteristics and their responsiveness to the tumor microenvironment or infection microenvironment [150]. In contrast to conventional metal oxides-based Fenton systems that rely heavily on endogenous H_2O_2 levels within tumors, metal peroxides intrinsically contain peroxide bonds that can gradually generate H_2O_2 under both the weakly acidic tumor microenvironment and infection microenvironment. This enables a sustained ROS production mechanism without the need for externally supplied H_2O_2, thereby markedly improving CDT reaction kinetics and overcoming the therapeutic limitations associated with insufficient H_2O_2 concentration in tumor tissues [151,152].

Among the various peroxide sources applicable to biomedical therapy, CaO_2 is widely recognized as one of the materials most compatible with the tumor microenvironment and infection microenvironment owing to its combination of stability, biocompatibility, and controllable reactivity. Compared with other metal peroxides, CaO_2 exhibits greater chemical stability under neutral conditions and pronounced pH responsiveness—it remains relatively inert in neutral environments but rapidly decomposes in acidic microenvironment (tumor microenvironment and infection microenvironment) to generate H_2O_2, followed by the release of O_2, thus serving simultaneously as a sustained peroxide and oxygen source [153]. Moreover, the mild reaction behavior and easily tunable release rate of CaO_2 allow it to form stable and adjustable composite systems with a variety of carriers, ensuring continuous H_2O_2 supply while avoiding the systemic toxicity and uncontrolled reactions associated with direct H_2O_2 injection [154]. Its low cost, facile synthesis, and ease of encapsulation further contribute to its wide application. For example, Zhang et al. loaded CaO_2 onto $Ti_3C_2F_x$ to construct $CaO_2/Ti_3C_2F_x$ composites (Fig. 7(a)). Under ultrasonic irradiation, CaO_2 reacts with water to continuously generate exogenous H_2O_2; simultaneously, during ultrasonic stimulation, the newly produced H_2O_2 further reacts with $Ti_3C_2F_x$, promoting the formation of a certain amount of TiO_{2-x} on the material surface. This TiO_{2-x} phase, as a semiconductor containing coexisting Ti^{4+}/Ti^{3+} pairs (Fig. 7(b)), enables the composite to generate large quantities of $^1O_2$ via SDT while also producing ROS through Ti^{4+}/Ti^{3+} cycling in a CDT-like manner (Fig. 7(c)). Thus, the system exhibits dual CDT–SDT therapeutic characteristics. In addition, the continuous release of H_2O_2 from CaO_2 provides a persistent substrate supply, enabling effective tumor inhibition and antibacterial performance [155]. Similarly, Liu et al. modified $CaO_2/Ti_3C_2F_x$ with PVP, which not only enhanced the overall stability of the composite but also demonstrated excellent antibacterial activity and significant antitumor efficacy through combined CDT–SDT therapy [156]. Collectively, future incorporation of NIR irradiation could further enhance therapeutic outcomes by integrating CDT–SDT–PTT therapy and leveraging the excellent photothermal performance of MXene.

In addition to CaO_2-based systems, transition-metal peroxides offer distinct advantages in reaction behavior and reactive species generation. A key feature of these materials lies in the fact that, during their decomposition, transition-metal peroxides not only release H_2O_2 but also simultaneously liberate metal ions with specific valence states. These metal ions can directly participate in Fenton or Fenton-like reactions, undergoing cyclic redox interactions with endogenous or exogenous H_2O_2 to achieve more efficient ROS generation. In contrast to CaO_2, which serves solely as a peroxide source, such systems introduce additional catalytically active metal centers, thereby markedly enhancing electron-transfer kinetics, lowering reaction energy barriers, and strengthening H_2O_2 activation. This synergistic interplay significantly accelerates ROS production. In other words, these materials enable a dual cooperative mechanism by supplying both exogenous H_2O_2 and metal ions capable of continuous catalytic cycling [158]. This combined mechanism yields a pronounced amplifying effect on radical generation and confers superior reaction-kinetic advantages, ultimately contributing to enhanced therapeutic performance. For example, Liu et al. successfully loaded CuO_2 onto MXene to construct a $CuO_2/Ti_3C_2F_x$ composite. In the tumor microenvironment, the CuO_2 releases Cu^{2+} under acidic conditions, thereby activating Fenton-like reactions and efficiently generating ROS to kill tumor cell. Simultaneously, the decomposition process also produces H_2O_2 (Fig. 7(d)), helping to compensate for the insufficient endogenous H_2O_2 levels typical of tumor tissues and providing sustained substrate for successive redox reactions (Fig. 7(e)). Moreover, the MXene component exhibits strong photothermal conversion under NIR irradiation, supplying additional thermal energy to accelerate ROS production and release, ultimately enabling rapid and substantial accumulation of reactive oxygen species. Through this CDT–PTT synergistic mechanism, the $CuO_2/Ti_3C_2F_x$ composite demonstrates markedly enhanced tumor-killing efficacy and pronounced therapeutic outcomes in both in vitro and in vivo studies [157]. Similarly, Zhao et al. embedded $CuO_2/Ti_3C_2F_x$ composite particles into electrospun polycaprolactone (PCL) fiber membranes and applied them directly to wound sites. Under NIR irradiation, the MXene component membrane rapidly and effectively eliminates bacteria at the wound surface and mitigates local infection, thereby significantly promoting the wound-healing process [159].

Moreover, certain metal peroxides are capable of continuously releasing oxygen during their hydration or decomposition processes. This property enables them to partially alleviate the hypoxic conditions commonly present within the tumor microenvironment. By increasing the local oxygen concentration, these materials not only enhance the availability of oxygen molecules required for subsequent reactions and thereby promote efficient ROS generation, but also provide a more favorable reaction basis for oxygen-dependent therapeutic modalities such as SDT. Consequently, under the coupling of multiple mechanisms,

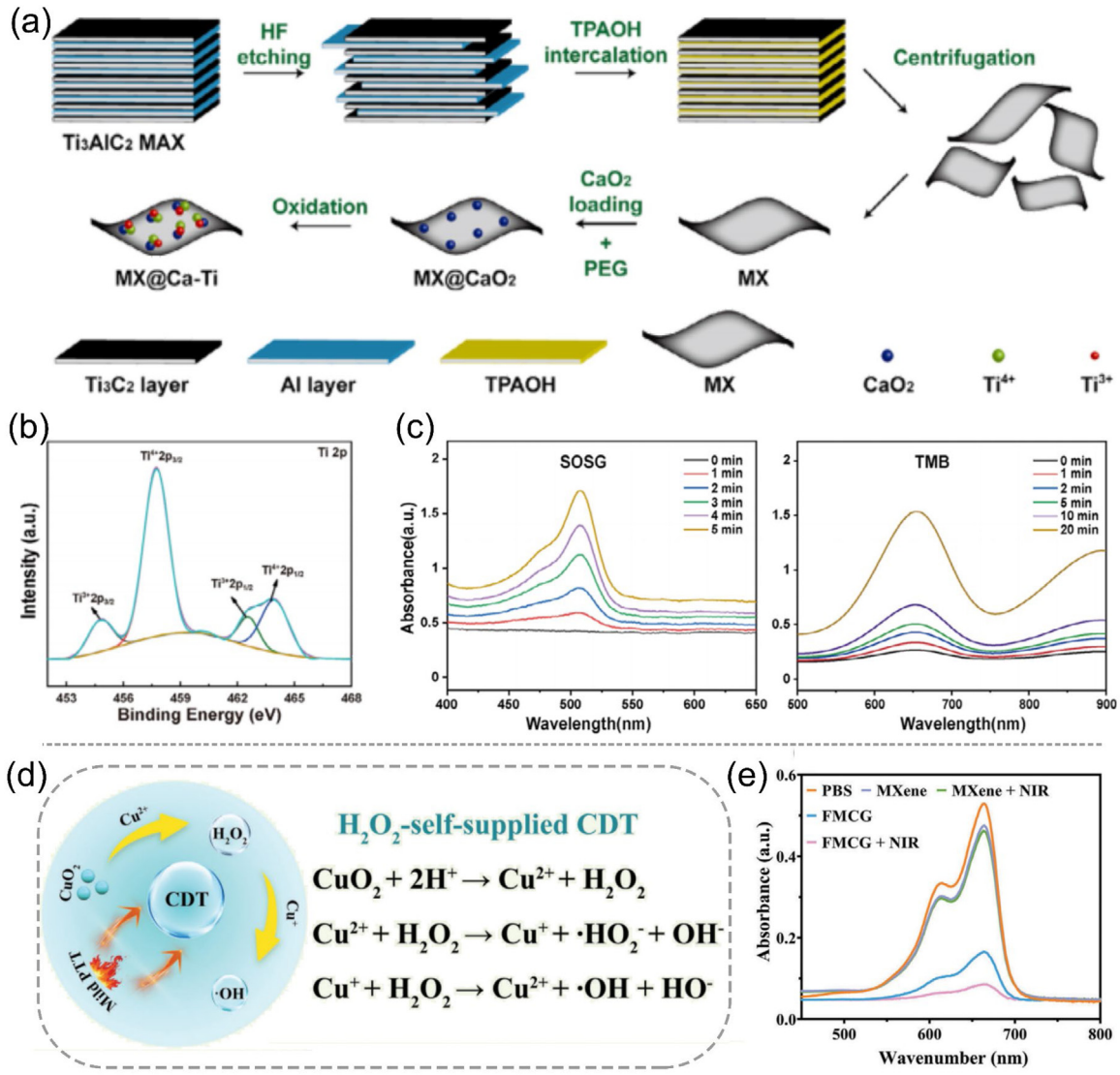

Fig. 7. (a) Schematic illustration of the synthesis of CaO_2/TiO_{2-x}/MXene; (b) Surface valence state distribution of Ti; (c) ROS generation capability [155]. Copyright 2025 Wiley-VCH. (d) schematic illustration of H_2O_2 self-supplied CDT in CuO_2/MXene, and (e) ROS generation capability of CuO_2/MXene [157]. Copyright 2024 Wiley-VCH.

such materials exhibit the potential to produce synergistic therapeutic effects.

4.5. Other MXene-based composites

In addition to the widely investigated MXene composite systems discussed above, a variety of other inorganic materials have also been incorporated with MXene to further expand its functional performance and application scope in biomedical therapy. Among these materials, selenides have attracted increasing attention owing to their excellent electron-transport capability, tunable valence states, and pronounced photothermal responsiveness. The localized heating generated through photothermal conversion, together with the intrinsic electronic characteristics of selenides, can jointly accelerate ROS generation during treatment. Moreover, certain selenide species are reported to induce a degree of immune activation, granting them a unique and valuable role within therapeutic systems [6]. For instance, Sun et al. constructed a $Cu_{2-x}Se/Ti_3C_2F_x$ composite by integrating $Cu_{2-x}Se$ onto the surface of $Ti_3C_2F_x$, achieving notable tumor eradication through combined CDT–PTT therapy, thereby highlighting the promising applicability of selenides in MXene-based synergistic platforms. However, the potential toxicity associated with selenium cannot be overlooked. High doses of Se, as well as free selenium species generated in vivo, may cause pronounced cytotoxicity or hepatotoxicity. Furthermore, some selenides are prone to oxidative decomposition under physiological conditions, producing toxic selenium oxoanions such as SeO_3^{2-} and SeO_4^{2-}, which raises significant biosafety concerns and limits their broader therapeutic translation [160].

Similar to selenides, sulfide-based materials have also been extensively explored as functional components in MXene-based therapeutic platforms. Sulfides, particularly transition-metal sulfides such as CuS and FeS_2, possess intrinsic catalytic activity and favorable electronic structures that enable Fenton or Fenton-like reactions under tumor TME conditions. When integrated with MXene, these sulfides can benefit from the high electrical conductivity and strong photothermal conversion efficiency of $Ti_3C_2F_x$. The localized hyperthermia generated by MXene under NIR irradiation not only induces direct tumor cell damage but also accelerates reaction kinetics and enhances ion release from sulfides, thereby promoting ROS generation and amplifying CDT efficacy. Representative examples include the $CuS/Ti_3C_2F_x$ system reported by Duan et al., in which Cu^{2+}/Cu^+ redox cycling under NIR irradiation significantly enhanced ROS production. Similarly, the $FeS_2/Ti_3C_2F_x$ composite developed by Deng et al., where Fe-mediated Fenton-like reactions were strengthened by photothermal heating, showed excellent catalytic

activity [156,158]. Both systems demonstrated remarkable tumor inhibition under CDT–PTT dual-modality therapy, underscoring the potential of sulfide-integrated MXene platforms for synergistic cancer treatment. Nevertheless, challenges similar to those observed for selenides persist. The in vivo degradation behavior and metabolic pathways of sulfide nanomaterials are not yet fully elucidated. Sulfides may undergo oxidation or ion dissolution under physiological conditions, leading to the release of sulfur-containing species, whose in vivo distribution, clearance routes, and cumulative toxicity require systematic investigation. These unresolved biosafety and pharmacokinetic issues present substantial barriers to clinical translation and highlight the necessity for more rigorous evaluation of degradation mechanisms, dose thresholds, and long-term biocompatibility.

Beyond these biosafety considerations, from a materials chemistry perspective, the fundamental origin of synergistic behavior of MXene-based sulfides and selenides composites requires deeper discussion. While synergistic therapeutic effects have been empirically observed, the integration of sulfides and selenides with MXene also raises important questions regarding interfacial electronic coupling and band alignment. Sulfides and selenides generally possess narrow band gaps and high carrier mobility, which may facilitate faster interfacial electron transfer and improved charge separation efficiency under external stimulation. When interfaced with metallic-conductive MXene substrates, the formation of Schottky-type contacts can modulate local electron density distribution, thereby influencing redox reaction kinetics and ROS generation pathways. Nevertheless, the same electronic flexibility that contributes to high therapeutic activity may also accelerate structural degradation under physiological conditions. The relatively weaker chemical bonds, compared with metal–oxygen bonds in oxides, render sulfides and selenides more susceptible to oxidation, especially in ROS-rich microenvironments. This intrinsic instability highlights a fundamental trade-off between redox reactivity and structural durability. More broadly, these observations suggest that the performance of MXene-based sulfides and selenides composites is not solely determined by the individual properties of each component, but rather by the dynamic electronic interactions established at the interface.

Overall, both sulfides and selenides can generate pronounced synergistic therapeutic effects when combined with MXene, yet they inevitably introduce a trade-off between therapeutic efficacy and biosafety. Therefore, future research should focus on enhancing structural stability and biocompatibility while maintaining high therapeutic performance [161,162]. Only by effectively balancing efficacy and safety can these composite systems achieve broader and more sustainable development in the field of biomedical therapy.

4.6. Comparative analysis of MXene-based nanozyme systems

Although various nanoplatforms have demonstrated excellent therapeutic performance, different nanozyme systems possess distinct characteristics and inherent limitations in specific applications. For instance, oxide-based composite systems benefit from the multivalent states of metal ions, which can facilitate Fenton cycling and thereby enhance CDT efficacy. However, the ratio between high- and low-valence metal species in oxides is often difficult to precisely control. As a result, batch-to-batch variations in nanozyme synthesis may lead to inconsistencies in therapeutic performance. Moreover, such valence fluctuations may also influence oxide-based composites primarily designed for PDT or SDT. Although the bandgap of oxides is theoretically tunable, variations in oxidation states during synthesis can lead to differences in surface defect density among batches. These defect variations may alter the bandgap structure and subsequently affect light or ultrasound absorption efficiency, ultimately causing fluctuations in the therapeutic outcomes of MXene-oxide nanozyme systems. Similar challenges may also arise in peroxide-, sulfide-, and selenide-based systems. In particular, metal peroxide composite systems can release exogenous H_2O_2 to supply substrates for Fenton reactions. However, during this process, MXene is inevitably oxidized, generating additional Fenton-active sites. The extent of this oxidation is highly environment-dependent and difficult to control, which further contributes to variability in therapeutic efficacy.

In contrast, metal-based systems (including nanoparticles and single atoms) and coordination-based systems (including molecular coordination complexes and MOF) generally feature more well-defined coordination environments around their active metal centers. Consequently, their therapeutic performance may exhibit improved reproducibility. Nevertheless, metal/MXene systems often rely on noble metals, which are costly. Furthermore, to optimize plasmonic resonance effects, the synthesis of noble metal nanoparticles typically requires the use of organic ligands or solvents to maintain specific morphologies. Residual organic species on the surface may introduce potential biotoxicity, thereby posing additional safety concerns. Similarly, in single-atom and metal–ligand composite systems, the incorporation of organic ligands or solvents is often unavoidable, potentially leading to comparable issues. By contrast, the synthesis of oxide composites frequently involves high-temperature calcination, which can effectively carbonize or eliminate residual toxic organic species. Therefore, although oxide-based composite systems may suffer from therapeutic variability, they may offer superior biosafety profiles.

Taken together, these comparisons indicate that the performance variability observed in MXene-based nanozymes is not merely material-specific, but fundamentally arises from the intrinsic coupling among valence-state regulation, defect chemistry, and active-site coordination environments. Fluctuations in any of these parameters can propagate through the interfacial electronic structure, thereby influencing catalytic kinetics, band structure stability, and reactive oxygen species generation efficiency. Importantly, optimization along one dimension—such as enhancing valence flexibility to promote Fenton cycling—may simultaneously introduce instability in defect distribution or coordination uniformity. This intrinsic interdependence explains why improvements in catalytic activity do not always translate into enhanced reproducibility across different composite systems.

Overall, different MXene-based nanozyme composite systems present distinct trade-offs between therapeutic stability, controllability, cost, and biosafety. Oxide systems offer structural robustness and potentially improved biocompatibility, yet they are more susceptible to valence-state fluctuations and defect variability, which may compromise batch-to-batch reproducibility. Peroxide-containing systems provide self-supplying Fenton substrates but introduce additional complexity through environment-dependent MXene oxidation. In contrast, metal nanoparticle, single-atom, and coordination-based systems exhibit more well-defined active-site structures and improved performance consistency; however, they often rely on noble metals and organic ligands, raising concerns regarding economic feasibility and potential biotoxicity. Therefore, future design strategies should aim to balance structural precision, synthetic controllability, therapeutic reproducibility, and biosafety, while minimizing cost and compositional complexity to facilitate clinical translation.

5. Summary and outlook

In this review, we have systematically summarized recent advances in MXene-based composite materials for multimodal biomedical therapy, emphasizing their unique physicochemical properties and multifunctional roles in energy conversion, interfacial electron regulation, and ROS generation. Owing to their metallic conductivity, tunable surface terminations, and two-dimensional layered structures, MXene provide versatile platforms for constructing tightly coupled heterostructures with enhanced charge transport and catalytic activity. Through rational integration with metal oxides, metallic nanoparticles, single-atom nanoenzymes, metal coordination compounds, MOF, and metal peroxides, diverse composite systems have been developed to achieve synergistic therapeutic effects.

Beyond serving as passive carriers or photothermal agents, MXene increasingly function as active electronic mediators that modulate interfacial energy band structure, promote directional electron transfer, suppress charge-carrier recombination, and accelerate redox reaction kinetics [163]. These capabilities enable amplified ROS production and improved energy utilization efficiency, forming the mechanistic basis for enhanced tumor ablation and antibacterial performance. Substantial progress has been achieved in structural engineering, mechanistic elucidation, and preclinical therapeutic validation, laying a solid materials and theoretical foundation for next-generation multimodal therapeutic platforms.

Nevertheless, despite these promising achievements, several fundamental scientific questions and translational barriers remain to be addressed before MXene-based systems can achieve widespread clinical application.

(i) Deepened mechanistic understanding for refined regulation of interfacial structure

Current research primarily focuses on therapeutic efficacy enhancement, whereas quantitative insights into interfacial electronic structures and energy conversion mechanisms remain insufficient. Although enhanced ROS production or photothermal efficiency is frequently reported, the fundamental electronic structure underlying these improvements are often not rigorously elucidated. A comprehensive understanding of band alignment, Fermi-level equilibration, interfacial dipole formation, built-in electric fields, and charge-carrier lifetime evolution is therefore essential for rational performance optimization. In particular, clarifying how interfacial electronic coupling governs charge separation efficiency, redox potential modulation, and catalytic kinetics will enable more deliberate and mechanism-driven material design rather than empirical trial-and-error approaches. Future investigations should combine advanced in situ characterization (e.g. X-ray absorption spectroscopy, electron paramagnetic resonance, transient absorption) with DFT calculations and multiscale simulations. Such combined experimental–theoretical approaches can provide real-time insights into electron transfer pathways, valence-state evolution, interfacial charge redistribution, and dynamic energy-flow processes under physiological conditions. Establishing quantitative structure–electronic property–ROS generation correlations will be crucial for transitioning from empirical material screening to predictive engineering, thereby enabling the rational design of MXene-based composites with controllable and optimized therapeutic performance.

(ii) Precise design and controllable activation of therapeutic synergies

Multimodal therapy should evolve beyond a simple additive combination of different treatment modalities. Instead of simply assembling multiple therapeutic functions into a single platform, an effective multimodal system should allow photothermal effects, ROS generation, and drug release to dynamically interact and amplify one another. This requires precise spatial and temporal regulation of photothermal conversion, catalytic ROS generation, drug release, and immune modulation to ensure that each modality is activated at the appropriate location and time point. Such synergistic effect is critical for amplifying therapeutic outcomes while avoiding unnecessary systemic toxicity. Rational heterostructure design, stimulus-responsive surface engineering, and programmable activation mechanisms should therefore be systematically explored to enable on-demand and feedback-regulated therapeutic responses. Additionally, external stimuli such as near-infrared irradiation, or ultrasound may be employed to dynamically modulate energy conversion and catalytic processes in real time. Through such integrated and precisely regulated strategies, therapeutic efficacy can be maximized, thereby improving clinical translational potential.

(iii) Biosafety, metabolic behavior, and long-term toxicity evaluation

Although short-term in vitro and in vivo studies generally demonstrate acceptable biocompatibility, the long-term metabolic behavior, degradation pathways, immunogenicity, and potential chronic toxicity of MXene-based composites remain inadequately understood. Gaps persist regarding their chronic metabolic trajectories, specific enzymatic or oxidative degradation pathways, and the potential for cumulative toxicity resulting from persistent retention. Given the inherent high surface reactivity and the susceptibility of the inorganic lattice to structural fragmentation or transformation within complex physiological microenvironments, it is imperative to conduct systematic investigations into their dynamic biodistribution and terminal clearance kinetics. Furthermore, the evolution of the bio-interface—specifically the formation and maturation of the protein corona—must be rigorously characterized, as it dictates subsequent immune recognition and inflammatory signaling. Establishing standardized, high-throughput evaluation protocols and employing hierarchically structured animal models will be indispensable for accurately delineating long-term safety profiles. Such rigorous toxicological frameworks are essential to address safety concerns and fulfill the stringent requirements of regulatory approval processes for clinical translation.

(iv) Scalable manufacturing and quality control

From a translational perspective, scalable synthesis and batch-to-batch consistency represent critical challenges that must be addressed to bridge the gap between laboratory research and clinical application. In current MXene-based systems, subtle variations in layer thickness, lateral size distribution, surface termination chemistry (–O, –OH, –F), defect density, and interlayer spacing can lead to significant deviations in electronic properties, interfacial charge transfer efficiency, and ultimately therapeutic performance. Such inconsistencies not only affect photothermal conversion and ROS generation but may also influence drug loading, release kinetics, and biodistribution in vivo, thereby posing a major barrier to reproducible therapeutic outcomes. Developing controllable and scalable etching methods, environmentally friendly synthesis strategies, and standardized post-treatment protocols—including precise control of oxidation state, surface functionalization, and structural uniformity—will be essential for producing MXene composites with predictable properties. In addition, high-throughput characterization techniques should be implemented. By integrating material quality standards with functional performance metrics, researchers can systematically correlate structural parameters with therapeutic efficacy. This approach enables rational optimization at scale. Beyond laboratory synthesis, the establishment of robust manufacturing protocols that ensure consistent layer number, defect density, and surface chemistry across batches is expected to facilitate industrial production and accelerate clinical translation. Ultimately, combining scalable fabrication strategies with stringent quality control will be a cornerstone for realizing the practical application of MXene-based multimodal therapeutic materials.

In summary, MXene-based composite materials continue to hold substantial promise in the field of multimodal biomedical therapy. With ongoing advances in materials engineering, mechanistic elucidation, and biomedical research, these systems are expected to play an increasingly important role in the development of efficient, low-toxicity, and controllable therapeutic strategies, while offering new paradigms and technological pathways for the broader field of multimodal.

Declaration of Competing Interest

The authors declare that they have no known competing financial interests or personal relationships that could have appeared to influence the work reported in this paper.

CRediT authorship contribution statement

Shilong Fu: Writing – review & editing, Writing – original draft, Conceptualization. **Huanyu Jin:** Writing – review & editing, Writing – original draft, Supervision, Funding acquisition. **Xu Xiao:** Writing – review & editing, Writing – original draft, Supervision, Funding acquisition.

Acknowledgements

This work was supported by the National Natural Science Foundation of China (52422205), National Key Research and Development Program of China (2023YFB3811303), the Natural Science Foundation of Sichuan Province (2026NSFSCZY0103).

References

[1] B. Yang, Y. Chen, J. Shi, Reactive oxygen species (ROS)-based nanomedicine, Chem. Rev. 119 (2019) 4881–4985, doi:10.1021/acs.chemrev.8b00626.
[2] B.L. Wang, S.Q. Hu, Y. Teng, J.L. Chen, H.Y. Wang, Y.Z. Xu, K.Y. Wang, J.G. Xu, Y.Z. Cheng, X. Gao, Current advance of nanotechnology in diagnosis and treatment for malignant tumors, Sig. Transduct. Target. Ther. 9 (2024) 200, doi:10.1038/s41392-024-01889-y.
[3] C. Holohan, S. Van Schaeybroeck, D.B. Longley, P.G. Johnston, Cancer drug resistance: An evolving paradigm, Nat. Rev. Cancer 13 (2013) 714–726, doi:10.1038/nrc3599.
[4] P. Vaupel, A. Mayer, Hypoxia in cancer: Significance and impact on clinical outcome, Cancer Metastasis Rev. 26 (2007) 225–239, doi:10.1007/s10555-007-9055-1.
[5] Y. Pu, B. Zhou, J. Bing, L. Wang, M. Chen, Y. Shen, S. Gao, M. Zhou, W. Wu, J. Shi, Ultrasound-triggered and glycosylation inhibition-enhanced tumor piezocatalytic immunotherapy, Nat. Commun. 15 (2024) 9023, doi:10.1038/s41467-024-53392-1.
[6] D. Wang, L. Ji, Y. Li, M. Xu, H. Wang, S. Brovelli, Z.Y. Qiao, J. Zhang, Y. Li, Iron–silver-modified quantum dots act as efficient catalysts in anti-cancer multitherapy through controlled, ultrasound-induced oxidation, Nat. Nanotechnol. 20 (2025) 1098–1107, doi:10.1038/s41565-025-01943-y.
[7] X. Zhu-Ge, D.M. Xi, S.S. Zhang, Multimodal tumor therapy based on chemodynamic therapy, Chin. J. Anal. Chem. 50 (2022) 100121, doi:10.1016/j.cjac.2022.100121.
[8] L. Zhang, Y. Fan, Z. Yang, C.Y. Wong, M. Yang, A novel reactive oxygen species nano-amplifier for tumor-targeted photoacoustic imaging and synergistic therapy, J. Colloid Interface Sci. 681 (2025) 331–343, doi:10.1016/j.jcis.2024.11.183.
[9] Y.F. Zhou, S.Y. Fan, L.L. Feng, X.L. Huang, X.Y. Chen, Manipulating intratumoral Fenton chemistry for enhanced chemodynamic and chemodynamic-synergized multimodal therapy, Adv. Mater. 33 (2021) 2104223, doi:10.1002/adma.202104223.
[10] X.W. Li, X.Y. Zhang, W.D. Zhang, L. Li, W.B. Gao, X.W. Zhang, D.W. Gao, Biocatalysis of MnO_2-mediated nanosystem for enhanced multimodal therapy and real-time tracking, ACS Sustain. Chem. Eng. 8 (2020) 13206–13214, doi:10.1021/acssuschemeng.0c02367.
[11] H. Wang, J. You, D. Shi, L. Cai, H. Shi, H. Shi, Multifunctional Ag_2S/g-C_3N_4 nanoparticles for photodynamic and photothermal cancer therapy under near-infrared excitation, ACS Appl. Nano Mater. 7 (2024) 19904–19914, doi:10.1021/acsanm.4c01221.
[12] S.X. Guan, T. Xu, J.Y. Zhang, Y.G. Luo, X. Zhai, N. Zhang, Y.Z. Fang, Q.F. Ke, Cu-MOFs based photocatalyst triggered antibacterial platform for wound healing: 2D/2D Schottky junction and DFT calculation, J. Hazard. Mater. 454 (2023) 131531, doi:10.1016/j.jhazmat.2023.131531.
[13] K. Huang, Z.J. Li, J. Lin, G. Han, P. Huang, Two-dimensional transition metal carbides and nitrides (MXenes) for biomedical applications, Chem. Soc. Rev. 47 (2018) 5109–5124, doi:10.1039/c7cs00838d.
[14] A. Lakmal, P.B. Thombre, C.E. Shuck, Solid-solution MXenes: Synthesis, properties, and applications, Accounts Chem. Res. 57 (2024) 3007–3019, doi:10.1021/acs.accounts.4c00387.
[15] K.R.G. Lim, M. Shekhirev, B.C. Wyatt, B. Anasori, Y. Gogotsi, Z.W. Seh, Fundamentals of MXene synthesis, Nat. Synth. 1 (2022) 601–614, doi:10.1038/s44160-022-00104-6.
[16] F. Wang, F. Tian, X.W. Xia, Z.Y. Pang, S.J. Wang, X. Yu, G.S. Li, Y.F. Zhao, Q. Xu, S. Hu, L. Ji, X.L. Zou, X.G. Lu, One-step synthesis of organic terminal 2D $Ti_3C_2T_x$ MXene nanosheets by etching of Ti_3AlC_2 in an organic Lewis acid solvent, Angew. Chem. Int. Ed. 63 (2024) e202405315, doi:10.1002/anie.202405315.
[17] W.Q. Li, G.Y. Xie, H.Y. Xu, Emerging trends in MXene research: Synthesis, process and hybrid with nanomaterials for biosensing, Coord. Chem. Rev. 531 (2025) 216493, doi:10.1016/j.ccr.2025.216493.
[18] W.J. Zhang, S.W. Li, V. Vijayan, J.S. Lee, S.S. Park, X. Cui, I. Chung, J. Lee, S.K. Ahn, J.R. Kim, I.K. Park, C.S. Ha, ROS- and pH-responsive polydopamine functionalized $Ti_3C_2T_x$ MXene-based nanoparticles as drug delivery nanocarriers with high antibacterial activity, Nanomaterials 12 (2022) 4392, doi:10.3390/nano12244392.
[19] S. Xu, B. Huang, H. Lin, J. Li, Z. Lu, Q. Zhang, J. Li, S. Yang, S. Lan, Y. Yang, Y. Feng, X. He, Iron/cobalt dual-atom catalyst orchestrate photothermal-chemodynamic immunotherapy against MRSA: Multi-omics dissection in murine and porcine models, Adv. Sci. (2025) e16783, doi:10.1002/advs.202516783.
[20] X. He, Z. Wang, B. Mao, H. Lin, X. Jin, M. Du, B. Huang, S. Xin, J. Qu, Y. Feng, Trimetallic Pt-Pd-Au alloy nanozymes for multimodal synergistic therapy to overcome deep-seated drug-resistant infections via ROS cascade, Bioact. Mater. 51 (2025) 841–857, doi:10.1016/j.bioactmat.2025.06.043.
[21] D. Wang, H. Jin, Y. Shen, D. Wang, J. He, J. Qu, X. He, Z. Jiang, NIR-II-activated iridium single-atom nanozymes for synergistic antibacterial therapy and tissue regeneration in MRSA-infected wounds and acute lung injury, Bioact. Mater. 51 (2025) 543–558, doi:10.1016/j.bioactmat.2025.05.022.
[22] M. Du, B. Huang, S. Xin, L. Wu, X. He, Atomic-engineered Ru single-atom-catalyst nanoplatforms with NIR-II-triggered oxidase-peroxidase cascades for bacterial pneumonia, Cell Rep. Phys. Sci. 6 (2025) 102870, doi:10.1016/j.xcrp.2025.102870.
[23] S.Y. Lin, M. Yang, J.J. Chen, W. Feng, Y. Chen, Y.F. Zhu, Two-dimensional $FePS_3$ nanosheets as an integrative sonosensitizer/nanocatalyst for efficient nanodynamic tumor therapy, Small 19 (2023) 2204992, doi:10.1002/smll.202204992.
[24] W.X. Fu, Y.Q. Cheng, W. Hu, J.H. Ling, X.K. Ouyang, N. Wang, Two-dimensional MXene nanosheets loaded with disulfiram for multimodal synergistic tumor photothermal-chemodynamic-chemotherapy, Mater. Today Commun. 48 (2025), doi:10.1016/j.mtcomm.2025.113490.
[25] N. Liu, Q.Q. Li, H.J. Wan, L.B. Chang, H. Wang, J.H. Fang, T.P. Ding, Q.Y. Wen, L.J. Zhou, X. Xiao, High-temperature stability in air of $Ti_3C_2T_x$ MXene-based composite with extracted bentonite, Nat. Commun. 13 (2022) 5551, doi:10.1038/s41467-022-33280-2.
[26] T.Z. Zhang, L.B. Chang, X.F. Zhang, H.J. Wan, N. Liu, L.J. Zhou, X. Xiao, Simultaneously tuning interlayer spacing and termination of MXenes by Lewis-basic halides, Nat. Commun. 13 (2022) 6731, doi:10.1038/s41467-022-34569-y.
[27] Z.C. Xi, H.L. Hu, Q. Chen, M.H. Ning, S.N. Wang, H.M. Yu, Y.M. Sun, D.W. Wang, H.Y. Jin, H.M. Cheng, 2D catalysts for electrocatalytic nitrate reduction and C-N coupling reactions, Adv. Funct. Mater. 35 (2025) 2425611, doi:10.1002/adfm.202425611.
[28] H.J. Wan, N. Liu, J. Tang, Q.Y. Wen, X. Xiao, Substrate-independent $Ti_3C_2T_x$ MXene waterborne paint for terahertz absorption and shielding, ACS Nano 15 (2021) 13646–13652, doi:10.1021/acsnano.1c04656.
[29] K. Yang, H.H. Huang, X.Q.Y. Zhang, M. Xin, F. Xiao, T.Z. Zhang, L.J. Zhou, X.F. Zhang, T. Zhao, X. Xiao, M. Hu, X. Yang, MXene-powered terahertz metamaterials as a real-time biosensing platform for in vivo thrombus monitoring, Adv. Mater. 38 (2025) e07063, doi:10.1002/adma.202507063.
[30] F. Gao, C. Xue, T. Zhang, L. Zhang, G.Y. Zhu, C.J. Ou, Y.Z. Zhang, X.C. Dong, MXene-based functional platforms for tumor therapy, Adv. Mater. 35 (2023) 2302559, doi:10.1002/adma.202302559.
[31] G.Y. Liu, J.H. Zou, Q.Y. Tang, X.Y. Yang, Y.W. Zhang, Q. Zhang, W. Huang, P. Chen, J.J. Shao, X.C. Dong, Surface modified Ti_3C_2 MXene nanosheets for tumor targeting photothermal/photodynamic/chemo synergistic therapy, ACS Appl. Mater. Interfaces 9 (2017) 40077–40086, doi:10.1021/acsami.7b13421.
[32] R.M. Ronchi, J.T. Arantes, S.F. Santos, Synthesis, structure, properties and applications of MXenes: Current status and perspectives, Ceram. Int. 45 (2019) 18167–18188, doi:10.1016/j.ceramint.2019.06.114.
[33] K. Hantanasirisakul, Y. Gogotsi, Electronic and optical properties of 2D transition metal carbides and nitrides (MXenes), Adv. Mater. 30 (2018) 1804779, doi:10.1002/adma.201804779.
[34] H.Y. Xia, B.Y. Li, Y.T. Ye, S.B. Wang, A.Z. Chen, R.K. Kankala, Transition metal oxide-decorated MXenes as drugless nanoarchitectonics for enriched nanocatalytic chemodynamic treatment, Adv. Healthc. Mater. 13 (2024) 2303582, doi:10.1002/adhm.202303582.
[35] L. Zhang, J. Liu, Y. Lv, Recent advances in reductive gas-augmented cancer photothermal therapy, Chem. Eng. J. 526 (2025) 170871, doi:10.1016/j.cej.2025.170871.
[36] S. Liang, Y. Liu, H. Zhu, G. Liao, W. Zhu, L. Zhang, Emerging nitric oxide gas-assisted cancer photothermal treatment, Exploration 4 (2024) 20230163, doi:10.1002/EXP.20230163.
[37] Z.M. Huang, X. Cui, S.L. Li, J.C. Wei, P. Li, Y.T. Wang, C.S. Lee, Two-dimensional MXene-based materials for photothermal therapy, Nanophotonics 9 (2020) 2233–2249, doi:10.1515/nanoph-2019-0571.
[38] H.Z. Lu, J.H. Wang, H.M. Li, W. Zhou, Q. Yuan, S. Liu, Efficient photothermal conversion of MXenes and their application in biomedicine, Mat. Chem. Front. 7 (2023) 4372–4399, doi:10.1039/d3qm00220a.
[39] X.Q. Fan, Y. Ding, Y. Liu, J.J. Liang, Y.S. Chen, Plasmonic $Ti_3C_2T_X$ MXene enables highly efficient photothermal conversion for healable and transparent wearable device, ACS Nano 13 (2019) 8124–8134, doi:10.1021/acsnano.9b03161.
[40] D. Xu, Z. Li, L. Li, J. Wang, Insights into the photothermal conversion of 2D MXene nanomaterials: synthesis, mechanism, and applications, Adv. Funct. Mater. 30 (2020) 2000721, doi:10.1002/adfm.202000712.
[41] Q.Q. Zhang, Z.C. Sun, Q.W. Guo, Y. Zhou, Z.Z. Li, J.Y. Wen, F.R. Li, Y.Y. Liu, S.Z. Jiao, Construction of excellent visible light absorption heat storage slurry using phase change microcapsules for solar thermal utilization, Chemistryselect 7 (2022) e202202124, doi:10.1002/slct.202202124.
[42] Y.L. Liu, W.Z. Geng, L.A. Wang, H.L. Wang, R. Zhang, D. Lan, B.B. Fan, Designing MXene hydrogels for flexible and high-efficiency electromagnetic wave absorption using digital light processing 3D printing, Chem. Eng. J. 505 (2025) 159489, doi:10.1016/j.cej.2025.159489.
[43] P. Zhu, Y. Pu, M. Wang, W. Wu, H. Qin, J. Shi, MnOOH-catalyzed autoxidation of glutathione for reactive oxygen species production and nanocatalytic tumor innate immunotherapy, J. Am. Chem. Soc. 145 (2023) 5803–5815, doi:10.1021/jacs.2c12942.
[44] S. Chen, F. Huang, L. Mao, Z. Zhang, H. Lin, Q. Yan, X. Lu, J. Shi, High Fe-loading single-atom catalyst boosts ROS production by density effect for efficient antibacterial therapy, Nano-Micro Lett. 17 (2024) 32, doi:10.1007/s40820-024-01522-1.
[45] B. Yang, J. Shi, Generalized concept of catalysis for chemical reactions: Nanocatalysis in medicine as a paradigm, Chem 11 (2025) 102549, doi:10.1016/j.chempr.2025.102549.
[46] L.Y. Yang, L. Shi, Y.H. Liu, Z.H. Liu, Z.J. Tian, H. Li, J.Y. Zhang, J. He, Y.M. Liu, ROS-mediated therapeutics combined with metal-based porphyrin nanoparticles and their applications in tumor treatment, Curr. Med. Chem. 32 (2025) 627–646, doi:10.2174/0109298673264765231006062032.
[47] Z.M. Tang, Y.Y. Liu, M.Y. He, W.B. Bu, Chemodynamic therapy: Tumour microenvironment-mediated Fenton and Fenton-like reac-

tions, Angew. Chem. Int. Ed. 58 (2019) 946–956, doi:10.1002/anie.201805664.
[48] L.H. Fu, Y.L. Wan, C. Qi, J. He, C.Y. Li, C. Yang, H. Xu, J. Lin, P. Huang, Nanocatalytic theranostics with glutathione depletion and enhanced reactive oxygen species generation for efficient cancer therapy, Adv. Mater. 33 (2021) 2006892, doi:10.1002/adma.202006892.
[49] Q. Zhang, J. Wang, Q. Yu, Q. Li, R. Fan, C. Li, Y. Fan, C. Zhao, W. Cheng, P. Ji, J. Sheng, C. Zhang, S. Xie, G. Henkelman, H. Li, Metal/MXene composites via in situ reduction, Nat. Synth. 4 (2024) 252–261, doi:10.1038/s44160-024-00660-z.
[50] A.P. Liu, Y. Liu, G.J. Liu, A.T. Zhang, Y.J. Cheng, Y. Li, L. Zhang, L.S. Wang, H. Zhou, J.Q. Liu, H.Y. Wang, Engineering of surface modified $Ti_3C_2T_x$ MXene based dually controlled drug release system for synergistic multitherapies of cancer, Chem. Eng. J. 448 (2022) 137691, doi:10.1016/j.cej.2022.137691.
[51] J.P. Ma, L. Zhang, B. Lei, Multifunctional MXene-based bioactive materials for integrated regeneration therapy, ACS Nano 17 (2023) 19526–19549, doi:10.1021/acsnano.3c01913.
[52] S. Liang, X. Xiao, L. Bai, B. Liu, M. Yuan, P.a. Ma, M. Pang, Z. Cheng, J. Lin, Conferring Ti-based MOFs with defects for enhanced sonodynamic cancer therapy, Adv. Mater. 33 (2021) e2100333, doi:10.1002/adma.202100333.
[53] P. Zhu, Y. Chen, J. Shi, Nanoenzyme-augmented cancer sonodynamic therapy by catalytic tumor oxygenation, ACS Nano 12 (2018) 3780–3795, doi:10.1021/acsnano.8b00999.
[54] Z. Li, B. Ding, J. Li, H. Chen, J. Zhang, J. Tan, X. Ma, D. Han, P.a. Ma, J. Lin, Multienzyme mimetic MoCu dual-atom nanozyme triggering oxidative stress cascade amplification for high-efficiency synergistic cancer therapy, Angew. Chem. Int. Ed. 64 (2024) e202413661, doi:10.1002/anie.202413661.
[55] Q. Bai, X. Lao, S.Y. Pang, Y. Zhao, Y. Liu, X.Y. Tian, J. Hao, Plaque-targeted delivery of fluoride-free MXene nanozyme for alleviating atherosclerosis via sonocatalytic therapy, Adv. Mater. 37 (2025) 2420189, doi:10.1002/adma.202420189.
[56] X. Li, Y. Tan, Z. Li, Y. Wang, C. Lu, S. Liao, B. Yin, B. Chen, H. Liu, H. Wei, G. Song, Cascade energy transformation in hybrid nanosensitizer enables ultrasound-activated luminescence imaging and enhanced sonodynamic therapy, J. Am. Chem. Soc. 147 (2025) 26518–26533, doi:10.1021/jacs.5c06434.
[57] B. Zheng, R. Zhang, F. Kuang, T. Hui, C. Fu, L. Zhang, C. Zhou, M. Qiu, B. Yue, Schottky heterojunction CeO_2@MXene nanosheets with synergistic type I and type II PDT for anti-osteosarcoma, J. Mater. Chem. A 12 (2024) 1816–1825, doi:10.1039/d3tb02835f.
[58] J.G. Jiang, X.Y. Lv, H.J. Cheng, D.L. Yang, W.J. Xu, Y.L. Hu, Y.N. Song, G.S. Zeng, Type I photodynamic antimicrobial therapy: Principles, progress, and future perspectives, Acta Biomater. 177 (2024) 1–19, doi:10.1016/j.actbio.2024.02.005.
[59] Y. Yin, X. Ge, J. Ouyang, N. Na, Tumor-activated in situ synthesis of single-atom catalysts for O_2-independent photodynamic therapy based on water-splitting, Nat. Commun. 15 (2024) 2954, doi:10.1038/s41467-024-46987-1.
[60] C. Liu, J.Z. Shao, J.H. Wang, Y.W. Wang, Y. Wang, Z.P. Fan, L.P. Li, G.S. Li, Construction of dynamic p-n junctions at atomic-scale for unanticipated photocatalytic oxidation activity, Appl. Catal. B-Environ. Energy 345 (2024) 123673, doi:10.1016/j.apcatb.2023.123673.
[61] S. Liu, K. Dou, B. Liu, M. Pang, P.a. Ma, J. Lin, Construction of multiform hollow-structured covalent organic frameworks via a facile and universal strategy for enhanced sonodynamic cancer therapy, Angew. Chem. Int. Ed. 62 (2023) e202301831, doi:10.1002/anie.202301831.
[62] J. Wang, P. Li, C. Liu, J. Liu, G. Li, L. Li, Recent advances in photothermal catalysis: Coupling hydrogen evolution and organic conversion, Int. J. Hydrog. Energy 67 (2024) 658–680, doi:10.1016/j.ijhydene.2024.04.161.
[63] N.H. Solangi, R.R. Karri, S.A. Mazari, N.M. Mubarak, A.S. Jatoi, G. Malafaia, A. Azad, MXene as emerging material for photocatalytic degradation of environmental pollutants, Coord. Chem. Rev. 477 (2023) 214965, doi:10.1016/j.ccr.2022.214965.
[64] H.S. Huang, Y. Song, N.J. Li, D.Y. Chen, Q.F. Xu, H. Li, J.H. He, J.M. Lu, One-step in-situ preparation of N-doped TiO_2@C derived from Ti_3C_2 MXene for enhanced visible-light driven photodegradation, Appl. Catal. B 251 (2019) 154–161, doi:10.1016/j.apcatb.2019.03.066.
[65] D.Q. Fan, Y. Lu, H. Zhang, H.L. Xu, C.H. Lu, Y.C. Tang, X.F. Yang, Synergy of photocatalysis and photothermal effect in integrated 0D perovskite oxide/2D MXene heterostructures for simultaneous water purification and solar steam generation, Appl. Catal. B 295 (2021) 120285, doi:10.1016/j.apcatb.2021.120285.
[66] H. Zhu, X. Zhang, Q. Wang, J. Deng, Z. Zhang, X. Zhang, J. Cao, B. He, In situ assembled titanium carbide-based heterojunctions for the synergistic enhancement of NIR-II photothermal/photodynamic therapy against breast cancer, J. Mater. Chem. A 10 (2022) 10083–10096, doi:10.1039/d2tb01783k.
[67] H. Wu, F. Wu, T. Zhou, Z. Hu, W. Wang, X. Liang, J. Wang, C. You, B. Sun, F. Lin, Activatable autophagy inhibition-primed chemodynamic therapy via targeted sandwich-like two-dimensional nanosheets, Chem. Eng. J. 431 (2022) 133470, doi:10.1016/j.cej.2021.133470.
[68] Y.C. Zhu, Y.L. Zhang, Y.L. Shen, S.J. Hong, K. Wang, X. Jia, W.G. Liu, Cu_2O-based core-shell nanostructures with glutathione depletion and O_2 generation properties for photodynamic/chemodynamic tumor therapy, ACS Appl. Nano Mater. 8 (2025) 12439-12439, doi:10.1021/acsanm.5c02626.
[69] S.T. Guan, R.S. Li, X.F. Sun, T. Xian, H. Yang, Construction of novel ternary Au/$LaFeO_3$/Cu_2O composite photocatalysts for RhB degradation via photo-Fenton catalysis, Mater. Technol. 36 (2021) 603–615, doi:10.1080/10667857.2020.1782062.
[70] F.F. Chai, K.Y. Li, C.S. Song, X.W. Guo, Synthesis of magnetic porous Fe_3O_4/C/Cu_2O composite as an excellent photo-Fenton catalyst under neutral condition, J. Colloid Interface Sci. 475 (2016) 119–125, doi:10.1016/j.jcis.2016.04.047.
[71] F. Jiang, B.B. Ding, S. Liang, Y.J. Zhao, Z.Y. Cheng, B.G. Xing, P.A. Ma, J. Lin, Intelligent MoS_2-CuO heterostructures with multiplexed imaging and remarkably enhanced antitumor efficacy via synergetic photothermal therapy/chemodynamic therapy/ immunotherapy, Biomaterials 268 (2021) 120545, doi:10.1016/j.biomaterials.2020.120545.
[72] F. Jiang, B.B. Ding, Y.J. Zhao, S. Liang, Z.Y. Cheng, B.G. Xing, B. Teng, P.A. Ma, J. Lin, Biocompatible CuO-decorated carbon nanoplatforms for multiplexed imaging and enhanced antitumor efficacy via combined photothermal therapy/chemodynamic therapy/chemotherapy, Sci. China-Mater. 63 (2020) 1818–1830, doi:10.1007/s40843-019-1397-0.
[73] Y.-J. Zhang, G.-D. Cheng, P. Suo, X. Chu, Y. Liu, S.L. Li, An infection microenvironment-responsive multifunctional nanocomposite for chronic wound treatment through redox homeostasis and macrophage regulation, Nanoscale 17 (2025) 19840–19853, doi:10.1039/d5nr01782c.
[74] Y. Wu, W. Xiong, Z. Wang, Y. Wang, K. Sun, X. Song, Z. Lv, W. Xu, W. Zhong, X. Zou, H. Cai, X. Wu, Self-assembled MXene-based Schottky-junction upon transition metal oxide for regulated tumor microenvironment and enhanced CDT/PTT/MRI activated by NIR irradiation, Chem. Eng. J. 427 (2022) 131925, doi:10.1016/j.cej.2021.131925.
[75] Z.C. Yang, C. Shan, J.J. Pignatello, B.C. Pan, Mn(II) acceleration of the picolinic acid-assisted Fenton reaction: New insight into the role of manganese in homogeneous Fenton AOPs, Environ. Sci. Technol. 56 (2022) 6621–6630, doi:10.1021/acs.est.1c08796.
[76] Y.C. Zhang, S.G. Hua, X.Q. Sun, Z.Y. Liu, Y. Dang, L. Zhang, Y.Z. Zhou, A novel electrochemical cathode based on sea urchin-like NiO/Co_3O_4 composite inducing efficient Fenton-like process for levofloxacin degradation, Appl. Catal. A 628 (2021) 118403, doi:10.1016/j.apcata.2021.118403.
[77] R.P. Ye, L.X. Ma, J.N. Mao, X.Y. Wang, X.L. Hong, A. Gallo, Y.F. Ma, W.H. Luo, B.J. Wang, R.G. Zhang, M.S. Duyar, Z. Jiang, J. Liu, A Ce-CuZn catalyst with abundant Cu/Zn-O_V-Ce active sites for CO_2 hydrogenation to methanol, Nat. Commun. 15 (2024) 2159, doi:10.1038/s41467-024-46513-3.
[78] Q.X. Zhou, A. Xing, J. Li, D.C. Zhao, K.F. Zhao, M. Lei, Synergistic enhancement in photoelectrocatalytic degradation of bisphenol A by CeO_2 and reduced graphene oxide co-modified TiO_2 nanotube arrays in combination with Fenton oxidation, Electrochim. Acta 209 (2016) 379–388, doi:10.1016/j.electacta.2016.05.094.
[79] R. Fiorenza, S.A. Balsamo, L. D'Urso, S. Scire, M.V. Brundo, R. Pecoraro, E.M. Scalisi, V. Privitera, G. Impellizzeri, CeO_2 for water remediation: Comparison of various advanced oxidation processes, Catalysts 10 (2020) 446, doi:10.3390/catal10040446.
[80] M. Tang, Y. Shi, L. Lu, J. Li, Z. Zhang, J. Ni, W. Wang, Y. Zhang, T. Sun, Z. Wu, Dual active nanozyme-loaded MXene enables hyperthermia-enhanced tumor nanocatalytic therapy, Chem. Eng. J. 449 (2022) 137847, doi:10.1016/j.cej.2022.137847.
[81] L. Zhao, R. Zhang, G. Yang, Y. Wang, S. Gai, X. Zhao, M. Huang, P. Yang, CeO_2 and glucose oxidase Co-enriched $Ti_3C_2T_x$ MXene for hyperthermia-augmented nanocatalytic cancer therapy, ACS Appl. Mater. Interfaces 16 (2024) 9968–9979, doi:10.1021/acsami.4c00425.
[82] R. Ma, S. Rao, J. Xie, C. Chen, C. Zhi, H. Chen, Q. Liu, J. Yang, In situ construction of vertical-TiO_2/MXene Schottky heterojunction with enhanced bacterial capture for synergistic photothermal and photocatalytic antibacterial effects, Appl. Surf. Sci. 710 (2025) 164011, doi:10.1016/j.apsusc.2025.164011.
[83] R. Zhang, W. Li, Z. Guo, Z. Chen, T. Wang, Y. Peng, A. Yu, D.S. Li, Q. Zhou, L. Niu, J. Tu, C. Sun, Q. Wu, Valence electron fluctuation in a high-entropy oxide heterojunction enables collaborative photodynamic and mild-thermal therapy for cutaneous biofilm infections, ACS Nano 19 (2025) 21348–21364, doi:10.1021/acsnano.4c18444.
[84] D.Y. Zhang, H. Liu, M.R. Younis, S. Lei, Y. Chen, P. Huang, J. Lin, In-situ $TiO_{(2-x)}$ decoration of titanium carbide MXene for photo/sono-responsive antitumor theranostics, J. Nanobiotechnol. 20 (2022) 53, doi:10.1186/s12951-022-01253-8.
[85] Y.K. Zhou, N.L. Yang, F. Gong, Y.J. Wang, X.Y. Yang, Y.Z. Dai, Q. Yu, L. Wang, W.F. Chen, M.P. Zhuo, L. Cheng, Oxygen-deficient tungsten oxide (WO_x) nanobelts with pH-sensitive degradation for enhanced sonodynamic therapy of cancer, ACS Nano 16 (2022) 17242–17256, doi:10.1021/acsnano.2c07903.
[86] Y.J. Wang, F. Gong, Z.H. Han, H.L. Lei, Y.K. Zhou, S.N. Cheng, X.Y. Yang, T.Y. Wang, L. Wang, N.L. Yang, Z. Liu, L. Cheng, Oxygen-deficient molybdenum oxide nanosensitizers for ultrasound-enhanced cancer metalloimmunotherapy, Angew. Chem. Int. Ed. 62 (2023) e202215467, doi:10.1002/anie.202215467.
[87] S. Chong, G.M. Zhang, Z.H. Wei, N. Zhang, T. Huang, Y.C. Liu, Sonocatalytic degradation of diclofenac with $FeCeO_x$ particles in water, Ultrason. Sonochem. 34 (2017) 418–425, doi:10.1016/j.ultsonch.2016.06.023.
[88] J. Xu, X. Wang, Y. Liu, Y. Li, D. Chen, T. Wu, Y. Cao, Interfacial engineering of Ti_3C_2-TiO_2 MXenes by managing surface oxidation behavior for enhanced sonodynamic therapy, Acta Biomater. 175 (2024) 307–316, doi:10.1016/j.actbio.2023.12.038.
[89] J. Xu, H.Y. Jin, T. Lu, J.S. Li, Y. Liu, K. Davey, Y. Zheng, S.Z. Qiao, $IrO_x{\cdot}nH_2O$ with lattice water-assisted oxygen exchange for high-performance proton exchange membrane water electrolyzers, Sci. Adv. 9 (2023) eadh1718, doi:10.1126/sciadv.adh1718.
[90] Y.T. Yan, J.H. Lin, K.K. Huang, X.H. Zheng, L. Qiao, S.D. Liu, J. Cao, S.C. Jun, Y. Yamauchi, J.L. Qi, Tensile strain-mediated spinel ferrites enable superior oxygen evolution activity, J. Am. Chem. Soc. 145 (2023) 24218–24229, doi:10.1021/jacs.3c08598.
[91] Y. Zhou, S.N. Sun, J.J. Song, S.B. Xi, B. Chen, Y.H. Du, A.C. Fisher, F.Y. Cheng, X. Wang, H. Zhang, Z.C.J. Xu, Enlarged Co-O covalency in octahedral sites leading to highly efficient spinel oxides for oxygen evolution reaction, Adv. Mater. 30 (2018) 1802912, doi:10.1002/adma.201802912.

[92] M.W. Ma, L.P. Li, X.B. Li, Q. Wang, T.T. Huang, Z.B. Geng, G. Tian, G.S. Li, Stabilization of unique $Zr^{>4+}$ species in $NiFe_2O_4$ nanocrystals for unprecedented catalytic transfer hydrogenation reaction, Appl. Catal. B: Environ. Energy 350 (2024), doi:10.1016/j.apcatb.2024.123905.
[93] G.C. Gao, G.S. Li, T.T. Huang, J.W. Wan, Z.B. Geng, H.T. Tang, X. Zhao, S.L. Fu, L.Y. Sun, J. Li, L.P. Li, Overcoming the activity-stability trade-off in electrocatalysts via unconventional two-step structural reconstructions of amorphous oxides, J. Am. Chem. Soc. 147 (2025) 29767–29778, doi:10.1021/jacs.5c04970.
[94] X. Zhao, Z.B. Geng, X.B. Li, J.Z. Shao, G.C. Gao, Z.Y. Shao, S.L. Fu, T.T. Huang, L.P. Li, G.S. Li, Capturing a transition phase during Birnessite-to-spinel transition for efficient water oxidation, J. Am. Chem. Soc. 147 (2025) 34361–34371, doi:10.1021/jacs.5c07103.
[95] T.L. Ho, C. Mutalik, L. Rethi, H.N.T. Nguyen, P.R. Jheng, C.C. Wong, T.S. Yang, T.T. Nguyen, B.W. Mansel, C.A. Wang, E.Y. Chuang, Cancer-targeted fucoidan-iron oxide nanoparticles for synergistic chemotherapy/chemodynamic theranostics through amplification of P-selectin and oxidative stress, Int. J. Biol. Macromol. 235 (2023) 123821, doi:10.1016/j.ijbiomac.2023.123821.
[96] Y.L. Yang, J.Q. Cen, J. Liu, Y.N. Liu, Iridium oxide-doped calcium phosphate nanoparticles for chemodynamic therapy of cancer, ACS Appl. Nano Mater. 6 (2023) 12447–12458, doi:10.1021/acsanm.3c02149.
[97] Y.F. Meng, D.S. Zhang, X. Chen, Z.C. Dai, X.X. Yao, P. Cui, D.X. Yu, G.R. Zhang, X.W. Zheng, FePt nanoparticles embedded in metal-organic framework nanoparticles for tumor imaging and eradication, ACS Appl. Nano Mater. 3 (2020) 4494–4503, doi:10.1021/acsanm.0c00581.
[98] G.N. Chen, Y.J. Ding, X.J. Hu, L. Yang, D.D. Zhao, Y.H. Kang, X.Z. Mou, C.J. Hou, Y. Cai, Biomimetic platinum-based nanoplatform for photoacoustic imaging-guided multimodal glioblastoma therapy, J. Colloid Interface Sci. 703 (2026) 139082, doi:10.1016/j.jcis.2025.139082.
[99] S. Ma, P. Yang, J. Chen, Z. Wu, X. Li, H. Zhang, NiCu alloys anchored Co_3O_4 nanowire arrays as efficient hydrogen evolution electrocatalysts in alkaline and neutral media, J. Colloid Interface Sci. 642 (2023) 604–611, doi:10.1016/j.jcis.2023.03.175.
[100] X. Chang, Q. Wu, Y. Wu, X. Xi, J. Cao, H. Chu, Q. Liu, Y. Li, W. Wu, X. Fang, F. Chen, Multifunctional Au modified Ti_3C_2-MXene for photothermal/enzyme dynamic/immune synergistic therapy, Nano Lett. 22 (2022) 8321–8330, doi:10.1021/acs.nanolett.2c03260.
[101] W.Y. Zhang, J.W. Liu, X.Y. Li, Y. Zheng, L.F. Chen, D.D. Wang, M.F. Foda, Z.Y. Ma, Y.L. Zhao, H.Y. Han, Precise chemodynamic therapy of cancer by trifunctional bacterium-based nanozymes, ACS Nano 15 (2021) 19321–19333, doi:10.1021/acsnano.1c05605.
[102] C. Lin, J.L. Li, X.P. Li, S. Yang, W. Luo, Y.J. Zhang, S.H. Kim, D.H. Kim, S.S. Shinde, Y.F. Li, Z.P. Liu, Z. Jiang, J.H. Lee, In-situ reconstructed Ru atom array on α-MnO_2 with enhanced performance for acidic water oxidation, Nat. Catal. 4 (2021) 1012–1023, doi:10.1038/s41929-021-00703-0.
[103] M. Tang, Z. Yue, J. Li, T. Sun, C. Chen, Nanozymes based on MXene nanosheets decorated with Pt nanoparticles for hyperthermal-enhanced cascade catalytic therapy of tumors, ACS Appl. Nano Mater. 6 (2023) 14609–14616, doi:10.1021/acsanm.3c03370.
[104] J. Peng, H. Liu, X. Tang, X. Cui, S. Li, X. Han, Cascade-catalytic MXene-AuPt nanozyme for photothermal-chemodynamic therapy and dual-mode imaging of breast cancer, Chin. J. Chem. 44 (2026) 291–302, doi:10.1002/cjoc.70335.
[105] D. Jana, D.D. Wang, A.K. Bindra, Y. Guo, J.W. Liu, Y.L. Zhao, Ultrasmall alloy nanozyme for ultrasound- and near-infrared light-promoted tumor ablation, ACS Nano 15 (2021) 7774–7782, doi:10.1021/acsnano.1c01830.
[106] Y.S. Zhao, S.Q. Zhao, Y. Du, Z.F. Gao, Y.L. Li, H.M. Ma, H. Li, X. Ren, Q. Fan, D. Wu, Q. Wei, Inverse oxide/alloy-structured nanozymes with NIR-triggered enzymatic cascade regulation of ROS homeostasis for efficient wound healing, Adv. Mater. 37 (2025) 2418731, doi:10.1002/adma.202418731.
[107] X. Hu, Z. An, W. Wang, X. Lin, T.S. Chan, C. Zhan, Z. Hu, Z. Yang, X. Huang, L. Bu, Sub-monolayer SbO_x on PtPb/Pt nanoplate boosts direct formic acid oxidation catalysis, J. Am. Chem. Soc. 145 (2023) 19274–19282, doi:10.1021/jacs.3c04580.
[108] Y.L. Zhong, B.B. Wang, K.F. Chu, A.J. Wang, T.J. Zhao, J.J. Feng, High-entropy intermetallic alloy/carbon nanoflower cascade nanozyme for multimodal synergistic cancer therapy, J. Colloid Interface Sci. 701 (2026) 138753, doi:10.1016/j.jcis.2025.138753.
[109] C.Y. Zhang, Z.G. Leng, Y.F. Wang, L. Ran, X. Qin, H. Xin, X.T. Xu, G.L. Zhang, Z.W. Xu, PDGFB targeting biodegradable FePt alloy assembly for MRI guided starvation-enhancing chemodynamic therapy of cancer, J. Nanobiotechnol. 20 (2022) 264, doi:10.1186/s12951-022-01482-x.
[110] Y. Liang, C. Liao, X. Guo, G. Li, X. Yang, J. Yu, J. Zhong, Y. Xie, L. Zheng, J. Zhao, RhRu alloy-anchored MXene nanozyme for synergistic osteosarcoma therapy, Small 19 (2023) e2205511, doi:10.1002/smll.202205511.
[111] H.Y. Li, J.M. Zhai, Q.N. Zhang, J.H. Li, Core-shell bimetallic alloyed Pd@Pt nanocubes for synergistic photothermal/chemodynamic infectious wound therapy, Colloids Surf., A 719 (2025) 137075, doi:10.1016/j.colsurfa.2025.137075.
[112] L.D. Liu, H.F. Zhang, S. Xing, Y. Zhang, L. Shangguan, C. Wei, F. Peng, X.Y. Liu, Copper-zinc bimetallic single-atom catalysts with localized surface plasmon resonance-enhanced photothermal effect and catalytic activity for melanoma treatment and wound-healing, Adv. Sci. 10 (2023) 2207342, doi:10.1002/advs.202207342.
[113] L. Zhang, C.J. Jiang, B. Li, Z.W. Liu, B.X. Gu, S.M. He, P.L. Li, Y. Sun, S.L. Song, A core-shell Au@Cu_{2-x}Se heterogeneous metal nanocomposite for photoacoustic and computed tomography dual-imaging-guided photothermal boosted chemodynamic therapy, J. Nanobiotechnol. 19 (2021) 410, doi:10.1186/s12951-021-01159-x.
[114] J.L. Wang, Q.Q. Duan, M. Yang, B.Y. Zhang, L. Guo, P.C. Li, W.D. Zhang, S.B. Sang, Rapid controlled synthesis of gold-platinum nanorods with excellent photothermal properties under 808 nm excitation, Beilstein J. Nanotechnol. 12 (2021) 462–472, doi:10.3762/bjnano.12.37.
[115] P. Pandey, S. Kunwar, J. Lee, Solid state dewetting of Ag/Pt bilayers for the stronger localized surface plasmon resonance (LSPR) properties: The dynamic control of surface morphology and elemental composition of AgPt and Pt nanostructures by the auxiliary Ag layer, J. Alloy. Compd. 813 (2020) 152193, doi:10.1016/j.jallcom.2019.152193.
[116] L. Jiang, Z. Yu, W. Zhao, Z. Yang, Y. Peng, Y. Zhou, X. Lin, S. Jin, Self-assembled MXene-Au multifunctional nanomaterials with various shapes for label-free SERS detection of pathogenic bacteria and photothermal sterilization, Anal. Chem. 95 (2023) 1721–1730, doi:10.1021/acs.analchem.2c04975.
[117] X. He, Y. Lv, Y. Lin, H. Yu, Y. Zhang, Y. Tong, C. Zhang, Platinum nanoparticles regulated V_2C MXene nanoplatforms with NIR-II enhanced nanozyme effect for photothermal and chemodynamic anti-infective therapy, Adv. Mater. 36 (2024) e2400366, doi:10.1002/adma.202400366.
[118] J. Jin, S. Wu, J. Wang, Y. Xu, S. Xuan, Q. Fang, AgPd nanocages sandwiched between a MXene nanosheet and PDA layer for photothermally improved catalytic activity and antibacterial properties, Dalton Trans. 52 (2023) 2335–2344, doi:10.1039/d2dt03596k.
[119] J. Liang, S. Li, X. Liu, Y. Wan, Y. Xia, H. Shi, S. Zhang, H.L. Wang, G. Lu, G. Wu, Y. Huang, Q. Li, Gas-balancing adsorption strategy towards noble-metal-based nanowire electrocatalysts, Nat. Catal. 7 (2024) 719–732, doi:10.1038/s41929-024-01167-8.
[120] P. Zhan, J. Zhuang, S. Yang, X. Li, X. Chen, T. Wen, L. Lu, P. Qin, B. Han, Efficient electrosynthesis of urea over single-atom alloy with electronic metal support interaction, Angew. Chem. Int. Ed. 63 (2024) e202409019, doi:10.1002/anie.202409019.
[121] P.P. Yang, J. Tao, F.F. Chen, Y.Y. Chen, J.Q. He, K. Shen, P. Zhao, Y.W. Li, Multienzyme-mimic ultrafine alloyed nanoparticles in metal organic frameworks for enhanced chemodynamic therapy, Small 17 (2021) 2005865, doi:10.1002/smll.202005865.
[122] J. Kwon, S. Sun, S. Choi, K. Lee, S. Jo, K. Park, Y.K. Kim, H.B. Park, H.Y. Park, J.H. Jang, H. Han, U. Paik, T. Song, Tailored electronic structure of Ir in high entropy alloy for highly active and durable bifunctional electrocatalyst for water splitting under an acidic environment, Adv. Mater. 35 (2023) e2300091, doi:10.1002/adma.202300091.
[123] A.L. Maulana, P.C. Chen, Z. Shi, Y. Yang, C. Lizandara-Pueyo, F. Seeler, H.D. Abruna, D. Muller, K. Schierle-Arndt, P. Yang, Understanding the structural evolution of IrFeCoNiCu high-entropy alloy nanoparticles under the acidic oxygen evolution reaction, Nano Lett. 23 (2023) 6637–6644, doi:10.1021/acs.nanolett.3c01831.
[124] B.T. Qiao, A.Q. Wang, X.F. Yang, L.F. Allard, Z. Jiang, Y.T. Cui, J.Y. Liu, J. Li, T. Zhang, Single-atom catalysis of CO oxidation using Pt_1/FeO_x, Nat. Chem. 3 (2011) 634–641, doi:10.1038/nchem.1095.
[125] Y. Xiong, J. Dong, Z.Q. Huang, P. Xin, W. Chen, Y. Wang, Z. Li, Z. Jin, W. Xing, Z. Zhuang, J. Ye, X. Wei, R. Cao, L. Gu, S. Sun, L. Zhuang, X. Chen, H. Yang, C. Chen, Q. Peng, C.R. Chang, D. Wang, Y. Li, Single-atom Rh/N-doped carbon electrocatalyst for formic acid oxidation, Nat. Nanotechnol. 15 (2020) 390–397, doi:10.1038/s41565-020-0665-x.
[126] Y. Zeng, C. Li, B. Li, J. Liang, M.J. Zachman, D.A. Cullen, R.P. Hermann, E.E. Alp, B. Lavina, S. Karakalos, M. Lucero, B. Zhang, M. Wang, Z. Feng, G. Wang, J. Xie, D.J. Myers, J.P. Dodelet, G. Wu, Tuning the thermal activation atmosphere breaks the activity–stability trade-off of Fe–N–C oxygen reduction fuel cell catalysts, Nat. Catal. 6 (2023) 1215–1227, doi:10.1038/s41929-023-01062-8.
[127] X. Guo, H. Zhang, Y. Wang, Y. Yao, C. Xiao, K. Gu, J. Qi, Y. Zhou, Y. Yang, Z. Zhu, J. Li, Confining asymmetrically coordinated cobalt single-atoms/clusters on holey MXene for ultrafast Fenton-like catalysis, Angew. Chem. Int. Ed. 64 (2025) e202511266, doi:10.1002/anie.202511266.
[128] J.Q. Zhang, Y.F. Zhao, X. Guo, C. Chen, C.L. Dong, R.S. Liu, C.P. Han, Y.D. Li, Y. Gogotsi, G.X. Wang, Single platinum atoms immobilized on an MXene as an efficient catalyst for the hydrogen evolution reaction, Nat. Catal. 1 (2018) 985–992, doi:10.1038/s41929-018-0195-1.
[129] V. Ramalingam, P. Varadhan, H.C. Fu, H. Kim, D.L. Zhang, S.M. Chen, L. Song, D. Ma, Y. Wang, H.N. Alshareef, J.H. He, Heteroatom-mediated interactions between ruthenium single atoms and an MXene support for efficient hydrogen evolution, Adv. Mater. 31 (2019) 1903841, doi:10.1002/adma.201903841.
[130] B. Geng, J. Hu, X. He, Z. Zhang, J. Cai, D. Pan, L. Shen, Single atom catalysts remodel tumor microenvironment for augmented sonodynamic immunotherapy, Adv. Mater. 36 (2024) e2313670, doi:10.1002/adma.202313670.
[131] H. Xi, H. Gu, Y. Han, T. You, P. Wu, Q. Liu, L. Zheng, S. Liu, Q. Fu, W. Chen, Y. Gao, Y. Wang, P. Yin, Peroxidase-like single Fe atoms anchored on $Ti_3C_2T_x$ MXene as surface enhanced Raman scattering substrate for the simultaneous discrimination of multiple antioxidants, Nano Res. 16 (2023) 10053–10060, doi:10.1007/s12274-023-5739-2.
[132] Z. Li, D. Xu, Z. Deng, J. Yin, Y. Qian, J.T. Hou, X. Ding, J. Shen, X. He, Single-atom-catalyzed MXene-based nanoplatform with photo-enhanced peroxidase-like activity nanotherapeutics for staphylococcus aureus infection, Chem. Eng. J. 452 (2023) 139587, doi:10.1016/j.cej.2022.139587.
[133] X. Sun, D. Wang, S. Ma, M. Du, J. Wen, X. He, X. Jin, Photothermal-Boosted chemodynamic nanoplatforms via MXene supported Pt single-atom catalysts for synergistic MRSA eradication and infected wound regeneration, Chem. Eng. J. 512 (2025) 162627, doi:10.1016/j.cej.2025.162627.
[134] H. Yang, F. Li, S. Zhan, Y. Liu, T. Liu, L. Wang, W. Li, M.S.G. Ahlquist, S. Farid, R. Ge, J. Wang, M.T.M. Koper, L. Sun, Metal-hydroxyls mediate intramolecular proton transfer in heterogeneous O-O bond formation, Nat. Chem. 18 (2026) 335–344, doi:10.1038/s41557-025-01993-8.

[135] S.Y. Zhai, Z. You, J.S. Li, B.C. Zheng, X.Y. Zhao, W.Y. Jiang, D.N. Su, H.B. Wang, C.H. Han, K.D. Lu, Hybrid-ligand metal-organic frameworks enabling radio-radiodynamic-chemodynamic therapy primes checkpoint blockade immunotherapy in hypoxic tumors, ACS Nano 19 (2025) 30100–30114, doi:10.1021/acsnano.5c06188.

[136] X. Gao, Y. Guo, S. Wang, J. Li, H. Xin, Z. Zhou, F. Yang, M. Nie, F. Song, Y. Wang, C. Dai, Z. Wen, Atomic-level regulation of the coordination structure in single-atom Fe nanozymes for tumor catalytic therapy, J. Colloid Interface Sci. 703 (2026) 139085, doi:10.1016/j.jcis.2025.139085.

[137] F. Duan, Q. Jia, G. Liang, M. Wang, L. Zhu, K.J. McHugh, L. Jing, M. Du, Z. Zhang, Schottky junction nanozyme based on Mn-bridged Co-phthalocyanines and $Ti_3C_2T_x$ nanosheets boosts integrative type I and II photosensitization for multimodal cancer therapy, ACS Nano 17 (2023) 11290–11308, doi:10.1021/acsnano.2c12270.

[138] Q. Zeng, Y. Liu, Y. Hu, H. Zou, S. Zhao, Y. Zhang, H. Wang, D. Li, C. Deng, Injectable MXene@zinc phthalocyanine heterojunction engineered hydrogel with self-regulating ROS for single 808 nm-activated photodynamic/photothermal synergistic therapy in scar-reduced wound healing, Chem. Eng. J. 524 (2025) 169002, doi:10.1016/j.cej.2025.169002.

[139] C.K. Zhou, D. Wang, F. Lagunas, B. Atterberry, M. Lei, H.C. Hu, Z.R. Zhou, A.S. Filatov, D.E. Jiang, A.J. Rossini, R.F. Klie, D.V. Talapin, Hybrid organic-inorganic two-dimensional metal carbide MXenes with amido- and imido-terminated surfaces, Nat. Chem. 15 (2023) 1722–1729, doi:10.1038/s41557-023-01288-w.

[140] X. Liu, H. Xie, S. Zhuo, Y. Zhou, M.S. Selim, X. Chen, Z. Hao, Ru(II) complex grafted $Ti_3C_2T_x$ MXene nano sheet with photothermal/photodynamic synergistic antibacterial activity, Nanomaterials 13 (2023) 958, doi:10.3390/nano13060958.

[141] C. Shuai, Z. Yu, F. Qi, T. He, D. Zhang, X. Shuai, M. Yang, NIR-Plasmon enhanced MXene/Fe-MOFs composite scaffold for synergistic chemodynamic-photothermal antibacterial therapy in bone implants, ACS Appl. Bio Mater. 8 (2025) 7331–7343, doi:10.1021/acsabm.5c01000.

[142] H. Furukawa, K.E. Cordova, M. O'Keeffe, O.M. Yaghi, The chemistry and applications of metal-organic frameworks, Science 341 (2013) 1230444, doi:10.1126/science.1230444.

[143] J.R. Li, R.J. Kuppler, H.C. Zhou, Selective gas adsorption and separation in metal-organic frameworks, Chem. Soc. Rev. 38 (2009) 1477–1504, doi:10.1039/b802426j.

[144] H.L. Tian, M.Z. Zhang, G.X. Jin, Y. Jiang, Y.X. Luan, Cu-MOF chemodynamic nanoplatform via modulating glutathione and H_2O_2 in tumor microenvironment for amplified cancer therapy, J. Colloid Interface Sci. 587 (2021) 358–366, doi:10.1016/j.jcis.2020.12.028.

[145] Y.Y. Zhong, X.S. Li, J.H. Chen, X.X. Wang, L.T. Wei, L.Q. Fang, A. Kumar, S.Z. Zhuang, J.Q. Liu, Recent advances in MOF-based nanoplatforms generating reactive species for chemodynamic therapy, Dalton Trans. 49 (2020) 11045–11058, doi:10.1039/d0dt01882a.

[146] K. Zhang, X.D. Meng, Z. Yang, H.F. Dong, X.J. Zhang, Enhanced cancer therapy by hypoxia-responsive copper metal-organic frameworks nanosystem, Biomaterials 258 (2020) 120278, doi:10.1016/j.biomaterials.2020.120278.

[147] D.F. Wang, X.L. Qiu, L.H. Hao, Z.R. Fan, S.X. Wang, C.X. Li, P-selectin-targeted polyguluronate sulfate-copper peroxide nanomicelles for chemodynamic therapy of breast cancer, Int. J. Biol. Macromol. 283 (2024) 137818, doi:10.1016/j.ijbiomac.2024.137818.

[148] C.J. Ou, Y.W. Zhang, W. Ge, L.P. Zhong, Y. Huang, W.L. Si, W.J. Wang, Y.X. Zhao, X.C. Dong, A three-dimensional BODIPY-iron(iii) compound with improved H_2O_2-response for NIR-II photoacoustic imaging guided chemodynamic/photothermal therapy, Chem. Commun. 56 (2020) 6281–6284, doi:10.1039/d0cc01164a.

[149] S. Iravani, A. Zarepour, A. Khosravi, R.S. Varma, A. Zarrabi, Smart MXene-based microrobots for targeted drug delivery and synergistic therapies, Nanoscale 17 (2025) 9040–9056, doi:10.1039/d4nr05160b.

[150] Y.L. Ji, Y.Z. Zhang, J.Q. Lu, F. Gao, X.Y. Lv, X.Y. Qu, G.Y. Zhu, T. Tian, H. Pang, Y. Tian, X.C. Dong, Multifunctional hydrogel electronics for synergistic therapy and visual monitoring in wound healing, Adv. Healthc. Mater. 14 (2025) 2404723, doi:10.1002/adhm.202404723.

[151] S. Chatterjee, A. Rai, R. Patwardhan, R. Agrawal, P. Chandwadkar, D. Pal, S. Gorai, C. Acharya, A.D. Ballal, S.K. Sandur, D. Goswami, GSH-responsive metal-organic framework-based nanoplatform for combined chemo-hemodynamic therapy, ACS Appl. Nano Mater. 7 (2024) 8197–8211, doi:10.1021/acsanm.4c00787.

[152] D. Jeong, M. Karmakar, J.W. Huh, H.J. Cho, Ion interference strategy cooperated with cascade chemodynamic/gas/chemo therapeutic functions of Mn/Ca/Pt-installed hydrogel network for breast cancer treatment, Chem. Eng. J. 520 (2025) 165765, doi:10.1016/j.cej.2025.165765.

[153] H.X. Feng, X.F. Su, D.P. Hu, Y.F. Hui, H.X. Su, J.L. Jiang, R.Y. Ji, S.L. Li, Z.J. Lin, F.Q. Tang, Metal-organic framework-based self-powered chemodynamic therapy nanosystem: CaO_2@PCN-222(Fe) and its mixed matrix membranes for promoting infected wound healing, Inorg. Chem. 64 (2025) 13557–13568, doi:10.1021/acs.inorgchem.5c02508.

[154] Y.J. Liang, Z.M. Cai, Y.M. Tang, C.L. Su, L.Y. Xie, Y. Li, X.Q. Liang, H_2O_2 self-supply and Ca^{2+} overloading MOF-based nanoplatform for cascade-amplified chemodynamic and photodynamic therapy, Front. Bioeng. Biotechnol. 11 (2023) 1196839, doi:10.3389/fbioe.2023.1196839.

[155] C. Liu, H. Li, G. Sun, Y. Wang, J. Zhang, X. Huang, Y. Chen, X. Chen, X. Liu, Z. Jiao, S. Zhang, Triggering self-supplied nanocatalytic reaction on Ti_3C_2 MXene@CaO_2-TiO_{2-x} for synergistic oral cancer therapy, antibacterial infection, and bone regeneration, View 6 (2025) 20250031, doi:10.1002/viw.20250031.

[156] Y. Yu, H. Sun, Q. Lu, J. Sun, P. Zhang, L. Zeng, K. Vasilev, Y. Zhao, Y. Chen, P. Liu, Spontaneous formation of MXene-oxidized sono/chemo-dynamic sonosensitizer/nanocatalyst for antibacteria and bone-tissue regeneration, J. Nanobiotechnol. 21 (2023) 193, doi:10.1186/s12951-023-01933-z.

[157] P. Xiong, X. Wei, L. Zhou, W. Zhou, M. Li, Y. Ge, J. Zou, S. Peng, L. Jiang, L. Tian, Y. Liu, Near-infrared light-triggered MXene nanocomposite for tumor-specific mild photothermal-enhanced chemodynamic therapy, Adv. Funct. Mater. 34 (2024) 2405124, doi:10.1002/adfm.202405124.

[158] B.J. Liu, X.H. Wang, W. Yang, H.S. Peng, H.X. Zhang, H_2O_2 Self-supplying $CaO_2/CuO_2/Fe_3O_4$ nanoplatform for enhanced chemodynamic therapy of cancer cells, Chemnanomat 10 (2024) 202300540, doi:10.1002/cnma.202300540.

[159] M. Liu, W. Zheng, J. Yi, J. Li, J. Li, Y. Deng, F. Yuan, K. Liang, Z. Zhao, Synergistic photocatalysis and biochemical reactivity in MXene/CuO_2 nanofibrous membrane for enhanced sterilization and tissue regeneration in chronic skin wounds, Chin. Chem. Lett. 36 (2025) 111985, doi:10.1016/j.cclet.2025.111985.

[160] M. Lu, T. Zhang, Y. Yang, X. Lin, J. Huang, Y. Sun, T. Sun, MXene loaded with $Cu_{2-x}Se$ nanozyme for nanocatalytic tumor therapy, Chemistry 31 (2025) e202500574, doi:10.1002/chem.202500574.

[161] Y. Tang, R. Zhao, M. Yi, Z. Ge, D. Wang, Y. Jiang, G. Wang, X. Deng, FeS_2-modified MXene nanocomposite platform for efficient PTT/CDT/TDT integration through enhanced GSH consumption, J. Mater. Chem. B 12 (2024) 5194–5206, doi:10.1039/d3tb02612d.

[162] T. Su, Y. Zhang, Y. Chang, X. Lin, M. Dong, S. Wu, Z. Wang, N. Duan, Nanozyme meets pathogen: A M-MXene@CuS platform for triple-mode detection and synergistic inactivation of MRSA, Chem. Eng. J. 519 (2025) 165639, doi:10.1016/j.cej.2025.165639.

[163] Y. Fei, Q. Wang, F. Wang, G. Zhang, M. Hu, T. Ding, T. Zhao, X. Xiao, M-site dependent terahertz intrinsic absorption in MXenes, InfoMat 7 (2025) e12654, doi:10.1002/inf2.12654.